Hydrocarbon-Seeded Ignition System for Small Spacecraft Thrusters Using Ionic Liquid Propellants

Stephen A. Whitmore, Daniel P. Merkley, and Shannon D. Eilers
Mechanical and Aerospace Engineering Department, Utah State University
4130 Old Main Hill, UMC 4130; (435)-797-2951
Stephen.Whitmore@USU.edu

Terry L. Taylor
Technology Development and Transfer Office,
NASA Marshall Spaceflight Center,
ZP-30, MSFC AL 35812; (256)-544-5916
Terry.Taylor@NASA.gov

ABSTRACT

"Green" propellants based on Ionic-liquids (*IL*s) like Ammonium DiNitramide and Hydroxyl Ammonium Nitrate have recently been developed as reduced-hazard replacements for hydrazine. Compared to hydrazine, *IL*s offer up to a 50% improvement in available density-specific impulse. These materials present minimal vapor hazard at room temperature, and this property makes IL's potentially advantageous for "ride-share" launch opportunities where hazards introduced by hydrazine servicing are cost-prohibitive. Even though *IL*s present a reduced hazard compared to hydrazine, in crystalline form they are potentially explosive and are mixed in aqueous solutions to buffer against explosion. Unfortunately, the high water content makes IL-propellants difficult to ignite and currently a reliable "cold-start" capability does not exist. For reliable ignition, *IL*-propellants catalyst beds must be pre-heated to greater than *350 C* before firing. The required preheat power source is substantial and presents a significant disadvantage for SmallSats where power budgets are extremely limited. Design and development of a "micro-hybrid" igniter designed to act as a "drop-in" replacement for existing *IL* catalyst beds is presented. The design requires significantly lower input energy and offers a smaller overall form factor. Unlike single-use "squib" pyrotechnic igniters, the system allows the gas generation cycle to be terminated and reinitiated on demand.

INTRODUCTION

This paper details the development and testing of a novel ignition system that is ideally suited for propellants based on Ionic-liquids (*ILs*). IL-based propellants have recently emerged as likely "reduced-hazard" candidates to replace hydrazine as a primary propellant for space propulsions systems. Compared to hydrazine, *IL*s offer up to a 50% improvement in available density-specific impulse. These materials present minimal vapor hazard at room temperature, and this property makes IL's potentially advantageous for "ride-shares" launch opportunities where hazards introduced by hydrazine servicing are cost-prohibitive.

Even though *IL*s present a reduced hazard compared to hydrazine, in crystalline form they are potentially explosive and are mixed in aqueous solutions to buffer against explosion. Unfortunately, the high water content makes IL-propellants difficult to ignite and currently a reliable "cold-start" capability does not exist. For reliable ignition, existing catalyst beds for *IL*-propellants must be pre-heated to greater than *350 C* before firing. The required preheat power source is substantial and presents a significant disadvantage for SmallSats where power budgets are extremely limited.

The proposed ignition technology is offered as a "drop-in" replacement for existing *IL* catalyst beds, and eliminates the need for a large pre-heat power source. The technology requires significantly lower input energy and offers a smaller overall form factor. Unlike single-use "squib" pyrotechnic igniters, the system allows the gas generation cycle to be terminated and reinitiated on demand. When fully developed the system will allow reliable IL-propellant ignition without a high wattage power source, toxic pyrophoric ignition fluids, or a bi-propellant spark ignitor.

The approach is fundamentally different from all other "green propellant" solutions in the aerospace in the industry. Although the proposed system is more correctly a "hybrid" rocket technology, since only a single propellant feed path is required, it retains all the simple features of a monopropellant system. The technology is based on the principle of "seeding" an oxidizing flow with a small amount of hydrocarbon.[1] The ignition is initiated electrostatically with a low-wattage inductive spark. Combustion gas byproducts from the hydrocarbon-seeding ignition process can exceed 2400 C and the high exhaust temperature ensures reliable propellant ignition. The system design is described in detail in this report.

BACKGROUND AND LITERATURE REVIEW

This section will discuss the current state of the art for hydrazine-based monopropellant systems, and motivate the need for "green" alternatives. Current state-of-the-art options will be considered, and the operational readiness for these options will be described. A thorough literature review of several promising "green" monopropellant options will be presented. Issues associated with operational readiness of the most promising options will be discussed.

Current State of the Art for Space Monopropellants

Hydrazine (N_2H_4) is by far the most commonly used propellant for primary spacecraft propulsion and attitude control thrusters. Hydrazine thrusters, which typically consist of an electric solenoid valve, a pressurant tank, and a catalyst bed of alumina pellets impregnated with iridium (Shell 405®)[2], feature simple design architectures, are highly reliable, and offer vacuum specific impulse (I_{sp}) exceeding 220 seconds. In a typical design, the catalyst initiates an exothermic decomposition of the hydrazine to produce ammonia, nitrogen, and hydrogen gases with approximately *1600 J/g* of heat released. Although hydrazine decomposition using the Shell 405 catalyst can be performed without additional heat input to the catalyst, typical designs pre-heat the catalyst bed to insure reliable ignition and a consistent burn profile.

Unfortunately, hydrazine is a powerful reducing agent that poses serious environmental concerns. Hydrazine is extremely destructive to living tissues and is a probable human carcinogen. Exposure produces a variety of adverse systemic effects including damage to liver, kidneys, nervous system, and red blood cells.[3] In addition to these biological and toxicological impacts, hydrazine presents significant environmental dangers for the spacecraft and launch vehicle.[4,5] When heated rapidly or exposed to extreme shock, such as the nearby explosion of a linear charge or blasting cap, hydrazine detonation is possible. Linear charges and explosive bolts are common on launch vehicles and spacecraft, thus the presence of hydrazine presents a tangible risk. Solid hydrazine buildup, possibly augmented by frozen oxygen, detonated by a linear charge in an adapter ring is suspected in the failure of an Atlas-Centaur upper stage.[6]

Most significantly, hydrazine has a high vapor pressure at room temperature, approximately 1000 kPa (145 psia). Because of this higher vapor pressure, hydrazine fumes significantly at room temperature and presents a high risk as a respiratory hazard. All hydrazine-servicing operations must be performed with the use of Self Contained Atmospheric Protective Ensemble (SCAPE) suits. Servicing using SCAPE personal protective equipment (PPE) is logistically complex and often adds considerable length to payload processing time.

On the Need for Reduced Toxicity, Reduced Hazard Replacements for Hydrazine

Although procedures are in place to allow hydrazine to be managed safely at tightly controlled government or defense-contractor operated test reservations and launch facilities, the toxicity and explosion potential of hydrazine requires extreme handling precautions that drive up operating costs. Increasingly, with a growing regulatory burden, infrastructure requirements associated with hydrazine transport, storage, servicing, and clean up of accidental releases are becoming cost prohibitive. As SmallSat operations continue to shift from government–run organizations to private companies and universities operating away from government-owned test reservations, servicing payloads requiring hydrazine as a propellant becomes operationally infeasible. Additionally, these extreme handling precautions generally do not favor hydrazine as a propellant for secondary payloads.

A recent study by the European Space Agency's European Space Research and Technology Center (ESA/ESTEC) has identified two essential design elements to achieving low cost space access; *1) Reduced production, operational, and transport costs due to lower propellant toxicity and explosion hazards, and 2) Reduced costs due to an overall reduction in subsystems complexity and overall systems interface complexity.*[8,9] This study showed the potential for considerable operational cost savings by simplifying propellant ground handing and servicing procedures. A non-toxic, stable "green" alternative for hydrazine is recommended by the study.

The ESA/ESTEC recommendations are directly aligned with NASA's In-Space Propulsion Systems Roadmap (ISPSR) TA02.1.1.1, *Monopropellants*.[10] A key element of ISPSR, identifies difficulties associated with hydrazine as a spacecraft propellant and recommends development of "*less hazardous, less toxic"* alternatives. NASA recently awarded a $40M contract to a team lead by Ball Aerospace Corporation for a Technology Demonstration Mission (TDM) to space-test a thruster system based on AF-M315E.[11] AF-M315E is a USAF-proprietary Hydroxylammonium Nitrate (HAN)-based IL propellant blend.[12]

Hydrazine Replacement Monopropellant Options

A useful monopropellant replacement for hydrazine must be sufficiently energetic to easily decompose and produce good combustion properties. Non-storable cryogenic or high freezing point propellants requiring temperature control are not appropriate for space propulsion applications. For SmallSat applications, even though mass-specific impulse is important, volume-specific impulse *(density impulse)* is an even more important consideration; and a high propellant storage density is preferred. Most importantly, candidate replacements for hydrazine must be sufficiently chemically and thermally stable to allow

storability, and also allow technicians and engineers to safely work with the propellant.

Hydrogen Peroxide (H_2O_2) is sometimes used as an oxidizing agent for bipropellant systems, and is currently being proposed as a "less toxic" alternative to hydrazine.[13] Unfortunately, H_2O_2 offers a significantly lower overall performance than hydrazine with a vacuum I_{sp} slightly below 170 seconds. More importantly, propulsion-grade solutions of H_2O_2 have an even higher room temperature vapor pressure than hydrazine -- approximately 1200 kPa (175 psia). Thus, while not as toxic as hydrazine, peroxide still presents a significant respiratory hazard. Propellant grade peroxide solutions are also unstable and present a moderate explosion risk.[14] The reduced performance, coupled with the still significant objective and health hazards, do not favor hydrogen peroxide as a "green" alternative to hydrazine.

For the past 15 years, the US Department of Defense (DoD) and the Swedish Space Corporation (SSC) subsidiary *ECological Advanced Propulsion Systems* (ECAPS) have been pursuing green-propellant alternatives based on aqueous solutions of *ionic liquids*. Ionic liquids are water-soluble substances that normally exist in solid form at room temperature, but melt below the boiling point of water. When dissolved in water these materials exhibit very strong ion-to-ion interactions. Two the most promising ionic liquid propellant options are based on the ammonium salts Ammonium Dinitramide (*ADN*)[15,16] and Hydroxylammonium Nitrate (*HAN*). [17,18] *ADN* melts at approximately 90-93 C, and HAN melts at approximately 44-45 C.

In solid form, both ADN and HAN are highly energetic salts with both reducing and oxidizing components. Consequently, in solid form both materials are unstable and potentially explosive. Thus both ADN and HAN are used in concentrated aqueous solutions for propellant applications in order to limit the explosion potential.[19] In typical applications, a fuel component like ethanol, glycine, or methanol is added to increase the propellant performance.

Because these propellants are mixed in aqueous solutions, they possess a very low vapor pressure at room temperature, and do not present a respiratory hazard. Thus, servicing operations can be performed with the use of SCAPE suits. This low vapor pressure is one of the primary reasons that these propellants are considered to be significantly less hazardous than either hydrazine or peroxide.

The manufacturing process for ADN was classified until 1989 when Bottaro, et al.[20] at the Stanford Research Institute (SRI) independently synthesized ADN.[22] Currently, ADN is manufactured and marketed commercially by EURENCO Bofors, of Karlskoga, Sweden. The Swedish Space Corporation (SSC) and the Swedish Defense Research Organization (FOI) have developed ADN into a liquid monopropellant. The liquid propellant blend is composed of an ionic aqueous solution (*10% water*) of ADN (*65%*) with methanol (*20%*) as a fuel, and ammonia (*5%*) as the solution stabilizer. This high performance green propellant is marketed under the product name LMP-103S by ECAPS, an SSC subsidiary. Moog Space and Defense Group and Alliant Techsystems (ATK) have partnered with ECAPS to make LMP-103S available to the US spacecraft market.[23]

The LMP-103S propellant blend is catalytically decomposed to produce water vapor and approximately 2000 J/g of heat output. In August 2011, ECAPS announced the results of a year-long series of in-space tests of a 1-N thruster comparing the performance of LMP-103S to hydrazine on the Prisma spacecraft platform. The comparisons claimed that LMP-103S delivered equivalent–to-superior performance. ECAPS has claimed that their 1-N thruster has achieved a TRL level of 7.0 following this spaceflight demonstration.[24,25,26]

The opportunity to fly the ADN- based system served as means to flight demonstrate the new propulsion technology, but also served as a demonstration of system level aspects for ADN-based propellants and their integration into spacecraft designs. Implementation of the 1-N ADN propulsion system solved issues with respect to five main system level interfaces; thermal, power, shock, vibration, and plume effects. ECAPS reported a mean in-space I_{sp} exceeding 220 seconds for the *Prisma* flight experiment.

The Naval Ordnance Station, Indian Head, MD developed a number of HAN-based liquid propellants for use in artillery guns for the US Army.[27] Three of these formulations, designated as LP1846, LP1845 and LP1898, were concentrated HAN mixed as an aqueous solution with tri-ethanol-ammonium nitrate (TEAN, $(OHCH_2CH_2)_3NHNO_3$) or diethyl-hydroxyl-ammonium nitrate (DEHAN, $(CH_3CH_2)_2NHOHNO_3$) as added components.[28,29,30,31] In these formulations, HAN serves as the oxidizing agent, the TEAN/DEHAN components act as fuel, and water is the solvent and buffering agent. The fuel components are added in the blend to achieve higher energy release and higher flame temperature. Of these propellant formulations, LP1846 was the most highly developed and tested.

Aerojet Corporation of Redmond Washington conducted alternative development activities where the fuel components of LP1846 were replaced with Glycine $(C_2H_5NO_2)$.[32] The Aerojet HAN-glycine (HANGLY26) formulation emphasized compatibility with existing hydrazine (S-405®) catalyst beds and was designed to produce a relatively low combustion temperature, approximately 1100 C. In this formulation sufficient water was added to keep the combustion temperature below 1100 C. This approach was selected to allow an up-front focus on propellant and thruster development rather than a lengthy catalyst development program.[33]

Because HANGLY26 decomposes with an exhaust

temperature similar to hydrazine, but produces exhaust products with a significantly higher molecular weight; HANGLY26 has a lower I_{sp} than hydrazine *(190 seconds)*. In its favor, HANGLY26 is significantly denser than hydrazine and produces greater volumetric impulse efficiency. Higher performing propellants that replace the glycine fuel component with methanol are under development. One formulation, designated as HAN269MEO, has achieved a vacuum I_{sp} near 270 seconds. Unfortunately, HAN269MEO burns considerably hotter than HANGLY26, and catalyst bed survivability is a significant issue.

With the TDM award to Ball Aerospace (Ref. 11) NASA has committed to AF-M315E as a "go-forward" green propellant option. The USAF Research Laboratory developed AF-M315E as proprietary a low-vapor pressure alternative to hydrazine. AF-M315E offers similar specific impulse (*Isp*) to hydrazine, and because of a substantially higher density provides up a 50% increase in density specific impulse. A series of broad characterization tests (Ref. 12) were performed and concluded that AF-M315E has attractive safety properties with significantly reduced toxicity compared to hydrazine. With the exception of ingestion, the propellant poses little personnel and environmental hazard and requires only minimal PPE for handling.

In hazard classification testing the propellant exhibited very benign reactions. Two package configurations were identified which showed no reaction to plastic explosive shock stimulus. Consequently, the US Department of Defense Joint Hazard Classifiers (JHC) and Department of Defense Explosives Safety Board (DDESB) have classified AF-M315E as a HD Class 1.3C material.

Current State of the Art for Ionic-Liquid Combustion Initiation

Unfortunately, because of the high water content, both LMP-103S and AF-M315E are notoriously hard to ignite. Multiple ignition methods including 1) pyrotechnic charges, 2) plasma torch, 3) electric spark plugs with bi-propellant oxidizer and fuel injectors, 4) pyrophoric ignition fluids, and 5) catalytically dissociation have been previously investigated.

Pyrotechnic or “squib” ignitors are capable of producing very high-enthalpy outputs; unfortunately these are one-shot devices and cannot be used for multiple motor ignitions. Pyrotechnic ignitors are most frequently used to ignite solid-propellant rockets where single-ignition capability is acceptable. For space-based propulsion systems requiring multiple restarts, these devices are unacceptable. Squib-based systems are also susceptible to the *Hazards of Electromagnetic Radiation to Ordnance* (HERO)[35], and pyrotechnic charges present a significant operations hazard for "rideshare" payloads.

Plasma torches are devices for generating a directed flow of plasma, and have been effectively used for gas turbine engines and supersonic combustion ramjets for ground test articles.[36] These devices produce very high output temperatures, but have a low total mass flow. Achieving a high-total enthalpy output requires a large input power. Typically, the power production units (PPU) these devices are bulky, and not generally amenable to SmallSat applications.

Bi-propellant ignitors are difficult to properly tune, and immediate ignition as the propellants enter the combustion chamber is essential. When liquid propellants fail to ignite within milliseconds after entering the chamber, excess propellants pool and can produce a “hard-start” where a large amount of gas is generated very rapidly at ignition. In a worst-case scenario, hard starts can cause the chamber to rupture catastrophically or at least fatigue the components to where a re-use is impossible. Ignitor flame holding stability is also a critical issue. Clearly, bi-propellant ignitors are capable of producing sufficient enthalpy to act as ignition sources for IL-propellants; however, the complexity required by the dual-propellant feed path, and potential stability-issues present significant operational disadvantages for small spacecraft.

Pyrophoric ignition fluids like Triethylaluminum-Triethylborane (TEA-TEB) are highly reliable, produce high output enthalpies, and can be used for multiple re-starts. Their use offers a very simple design solution. SpaceX originally considered a torch-ignitor for the Merlin Engine, but down-selected to TEA-TEB instead because of the complexity of the torch-ignition design, and the simplicity of the pyrophoric ignitor.[37] Historically, most LOX/RP engines, such as the Saturn V F-1, have used TEA-TEB as the ignition source. Unfortunately, like hydrazine, this class of propellants presents the extreme disadvantage of being highly toxic, potentially explosive, and hazardous to work with during ground processing. As mentioned previously, the 2003 ESA study (Ref. 9) strongly recommends against toxic and hazardous propellants, and the use of pyrophorics defeats the advantages of using IL-based propellants.

Thus, catalytic ignition remains the "method of choice" for IL-based propellants. Unfortunately; development of catalyst materials capable of withstanding the high combustion temperatures and required duty cycles remains a major challenge. The “holy grail” of a durable, highly active catalyst that can decompose IL-based propellants at low temperatures, but survive at high temperatures in an acidic and oxidizing environment, has yet to be achieved.

Reliable "cold-start" capability for ionic liquid propellants does not currently exist. For reliable ignition, existing catalyst beds for *IL*-propellants must be pre-heated to greater than *350 C* before firing. [38] This preheat requires a significant power source and presents a real disadvantage for SmallSats where power budgets are extremely limited.

Previous Catalyst Development for ADN and HAN-Based Green Propellants

ECAPS has developed a proprietary catalyst bed for decomposing the LMP-103S propellant, and this catalyst bed (*catbed*) has been demonstrated to be capable of surviving more than 30 minutes of collected burn time and multiple restarts. As mentioned previously, a major disadvantage of the ECAPS design is the requirement to preheat the catbed to at least 350 C before ignition can occur. For the *Prisma* flight, the maximum load during the catalyst pre-heating is 9.25 Watts, and 8.3 Watts during the thruster firing. Mean power consumption during firing is 7.3 watts. A 10-Watt heater was installed in the Prism spacecraft.

Depending on the relative sun angle, the duty cycle of the heater varies from 67 to 93%. The time required for 9.25 W *catbed* preheating to 340 C in flight varied from 600 s to 720 s. Operationally, preheating time is set conservatively to 30 minutes before enabling the thruster for firing. Because of the potential for freezing the water component of LMP-103S, the average temperature of the propellant tank was maintained at an operating temperature near 20 C. *Each ignition preheat cycle consumed as much as 25 kJ of energy. It is highly unlikely that a NanoSat-scale spacecraft could provide this sustained energy input.*

Zube and Wucherer[40] have developed a temperature resistant, Iridium-based catalyst for high performing HAN-mixtures that included HAN269MEO, and a HAN, aminoethylamine-trinitrate (TRN3), water mixture. Of primary interest in this effort was the development of the catalyst-support material to which an active Iridium catalyst is affixed. Two ceramics, zirconium diboride (ZrB_2) and zirconium carbide (ZrC), were found to be sufficiently robust to extend the test time to a point where the catalyst material was no longer the time limiting factor. These tests allowed significant burn times, greater than 5 minutes, and a large number of starts, greater than 20. Thus, for the first time, HAN thruster performance above *250 s* measured I_{sp} was achieved on a repeated basis without the handicap of frequent catalyst change. Unfortunately, like the ECAPS catbed, the iridium/zirconate catalysts still required a significant preheat, up to 400 C to achieve stable combustion.

Courthéoux et al. (2002)[41] used a batch reactor to investigate both thermal and catalytic decomposition of binary HAN/water solutions. A primary objective of this work was to investigate the effects of various catalyst bed architectures. In these tests Courthéoux and his team evaluated HAN/water solutions with different HAN concentrations of 20%, 60%, and 83% by weight. These 20%, 60%, and 83% solutions were shown to thermally dissociate at temperatures of 173 C, 170 C, and 135 C, respectively. In all cases the non-catalyzed HAN solution would not thermally dissociate until all of the water had vaporized and the liquid HAN droplets were allowed to come into close proximity. Two catbet architectures with platinum (*Pt*) deposited on alumina (Al_2O_3) and silica-doped alumina (Al_2O_3Si) were demonstrated to reduce the dissociation temperature of the 83% HAN solution to temperatures slightly above the sea-level-pressure boiling point of water, 110-115 C.

Recently, Oommen et al. (2011)[42] reproduced Courthéoux's results for HAN/water solutions using a catalyst with iridium-coated γ-alumina pellets. The experiments demonstrated that catalytic activity occurs at temperatures below the boiling point of water, even for aqueous blends containing low weight percentages of HAN. These tests demonstrated that catalytic HAN decomposition could occur with liquid water still present in the mixture.

Ren et al. (2006)[43], (2007)[44] investigated various precious metal catalysts and concluded that an Iridium/silicon-dioxide (Ir/SiO_2) catalyst was the most active and achieved ignition of an 80% HAN/water solution at room temperature (40 C). Even after 20 successive injections, the Ir/SiO_2 catalyst was still active. When the same catalyst was applied to HANGLY26, there was no catalytic activity at room temperature. When the catalyst was preheated by nitric acid, room temperature ignition of HANGLY26 was achieved, but with a significant ignition delay; however, it is very likely, that the nitric acid used to pre-heat the catalyst spontaneously reacted with the glycine to initiate the decomposition process, and that no actual catalysis occurred.

Ren et al. speculate that the lack of activity was due adsorption and site-blocking on the catalyst surface by the glycine component of the propellant mix. This result supports the general consensus that adding a fuel component to a binary HAN solution has the effect of increasing the solution stability, and makes the solution more difficult to decompose.

Other studies by Meinhart (Ref. 32) and Chang and Kuo[45] have verified that adding a fuel component has a stabilizing effect on HAN-propellant formulations. This added chemical stability significantly increases the required energy input energy for thermal decomposition and significantly reduces the reaction rate for the solution.

Electrolytic Decomposition of HAN-Based Propellants.

Several authors including Risha[46], Meng[47], Kare[48], and Kuo[49] have examined the electrolytic decomposition of HAN-based monopropellants. The motivation of these researchers was to circumvent many of the previously described difficulties with catalyst beds for IL-based propellants. Risha's initial experiments investigated the ignition characteristics of LP 1846 liquid propellant at room conditions using electrolysis. This study indicated that it is possible to initiate electrolytic HAN decomposition at near room temperature, but with a considerable time delay. The

time delay to peak power (reactivity) decayed exponentially from 160 seconds to 2-3 seconds with an increase in the input voltage from 7 to 12 VDC. Beyond 12 VDC, the time delay dependency became less significant and appeared to remain constant.

Meng and Kare followed up Risha's study with a study designed to develop detailed numerical models of the electrolytic dissociation process of HAN-based propellants. Their studies were conducted to investigate the effect of electric current, voltage, volume, initial temperature, and HAN concentration on the ignition time delay. Their results indicate that compared with the pure thermal decomposition process, electric current significantly enhances HAN decomposition. They predict that ignition time delay decreases with an increase in current, temperature, and increasing HAN concentration, and increases linearly with the volume of fluid being dissociated.

Kuo verified the predictions of Meng and Kare experimentally. Kuo also investigated the combined-electrolytic and catalytic ignition for HAN269MEO15 using the Shell 405® catalyst to establish the feasibility of room-temperature ignition. The electrolytic decomposition initiated the reaction and dominated at a lower temperature. As the temperature was increased, catalytic decomposition dominated the reaction. Combustion remained incomplete as indicated by the presence of *NO* and a much lower reaction temperature of 800 C compared to the adiabatic flame temperature of HAN269MEO15 of 1929 C. Significant delays were also experienced.

Wu, et al. (2008)[50] developed and tested a low temperature co-fired ceramic (LTCC) electrolytic-ignition HAN-based micro thruster. The microthruster was successfully ignited with an input of 45 volts, and a produced a thrust output of approximately *200 mN*. Energy input requirements and ignition delays were found dependent on the type of HAN-based propellant used, the voltage potential, and the size of the electrodes within the combustion chamber. Ignition was achieved with energy input as small as *1.9 Joules*, while ignition delays as short as 1/4th second were observed.

Wu's thruster design takes advantage of Kare's observation that ignition delays decrease linearly with the volume of fluid being decomposed (Ref. 47); thus very small electrolytic thrusters can be ignited with minimal ignition delays. When direct electrolytic decomposition at higher volumetric flow levels were attempted, long ignition delays result in accumulated pools of propellant in the catalyst bed making cold-starts unreliable.[51,52] As the thruster size grows to milli-Newton range, the required electrical power input became excessive. When sufficient power was input for rapid ignition, cracking of the thruster body was observed, and the thruster duty cycle lifetime was significantly reduced.

PROPOSED IL-PROPELLANT IGNITION ALTERNATIVE

The proposed alternative for igniting aqueous ionic liquid-based propellants builds on the work of Courthéoux (Ref. 41), Risha (Ref. 46), and Wu (Ref. 50). As mentioned previously, Courthéoux demonstrated that significant specific-energy input was required to thermally dissociate binary HAN/water solutions with up to 387 W/g/s of heating input rate input required for a 60% solution concentration. Even higher heat inputs are required to dissociate ternary solutions that include fuel components. Risha demonstrated that a significantly large power source is required if HAN-based propellants are to be dissociated without a long time delay. Thus, Wu's electrolytically ignited thruster design is limited to very small propellant mass flows and thrust levels.

The proposed ignitor design produces a very high power output, but is initiated using a low-wattage inductive spark. The design is adapted from a micro-hybrid thruster originally developed for stand-alone space propulsion applications. In this design a small section of solid Acrylonitrile Butadiene Styrene (*ABS*) thermoplastic acts as a seedling material to initiate combustion within an oxidizing flow. An inductive spark vaporizes a small amount of the solid *ABS* while the *oxidizer* flows across the fuel grain surface.

Although the process is relatively simple to implement technically, the chemistry of the *"hydrocarbon seeding"* process is extremely complex and a detailed physical model has yet to be developed. The authors believe that the spark-ablated *ABS* fuel "seeding vapor" plus residual energy from the spark are sufficient to trigger localized combustion along the surface of the porous ABS fuel grain. The heat released from this localized reaction in turn vaporizes more fuel and a sustained combustion reaction is rapidly achieved. Combustion exhaust byproducts have been measured to exceed 2400 C.[55]

Acrylonitrile Butadiene Styrene (ABS) as the Hydrocarbon Seeding Fuel Element

Multiple materials including Acrylic, Hydroxyl Terminated Polybutadiene (*HTBP*), PolyVinyl Vhloride (*PVC*), and *ABS* were investigated as potential materials for hydrocarbon seeding. It was discovered that *ABS* has several unique properties that make it the preferred material for this application. Although *ABS* burns with slightly less energy than the traditional legacy hybrid rocket fuel and solid-propellant binder *HTPB*; the combustion by-products have a lower molecular weight, and the resulting specific impulses are nearly identical. (Ref. 55)

Most importantly, unlike acrylic, *PVC* or *HTPB*, which are thermo-setting materials, *ABS* is an amorphous thermoplastic that softens and then melts in a highly predictable fashion when subjected to sufficient heat input. This property makes *ABS* the

materials of choice for a class of additive manufacturing known as Fused Deposition Modeling (FDM). Using FDM fabrication techniques, *ABS* plastics are readily shaped into complex geometries and it is possible to embed complex, high-surface area flow paths within the fuel grain.[23] These embedded flow paths cannot be achieved with thermosetting materials that are cast around mandrels and tooling that must be removed once the material is set.

ABS materials possess an extreme tolerance to harsh environmental conditions and have a very long, stable shelf life. Tests have shown that essentially no adverse out-gassing occurs under near-vacuum conditions. *ABS* is widely mass-produced for non-combustion applications including household plumbing and structural materials. More than 1.4 billion kg of *ABS* material were produced by petrochemical industries worldwide in 2010[18].

Because *ABS* melts before vaporizing when subjected to heat, a liquid film layer is produced along the length of the fuel port, and has the effect of providing both phase change and film cooling. This insulating layer directs the heat of combustion toward the nozzle exit, allowing the external motor case to remain cool during the burn.

ABS has a very high structural modulus (2.3 GPa) and tensile yield strength (40 MPa), approximately 38% of aluminum. In any design consideration, the relative strength and insulation properties of the ABS seeding material will allow the fuel element to take a significant portion of the ignition chamber pressure load which reduces the wall thickness requirements and the volumetric requirements for the system.

Finally, *ABS* plastic has a very high dielectric strength and can withstand up to *53.1 kV/mm*.[56] This dielectric value is significantly higher than air (*3 kV/mm*). When electrified charge builds up along the grain surface until a spark jumps along the fuel surface between thin gaps in the material and along built-up carbon on the surface. This spark locally ionizes the oxidizer flow, which reacts with the small amount of solid fuel vaporized from the surface (by the dissipated power). Residual energy from the spark initiates the combustion process. Figure 1 shows a high-tension inductive spark arcing across two small *ABS* test segments. The high dielectric stength of ABS allows multiple high-voltage sparks to be initiated without breaking down the material properties.

Hydrocarbon-Seeded Micro-hybrid Proof-of-Concept Prototype

A proof-of-concept prototype demonstrating the hydrocarbon-seeding process was built and tested by the authors of this paper in the Propulsion Test Laboratory at Utah State University. Figure 2 shows an exploded view of the prototype unit. The figure includes a standard AA battery for scale. The proof-of-concept design used gaseous oxygen (*GOX*) as the working fluid, and operated at 860 kPa (125 psia) chamber pressure with an oxidizer mass flow of approximately *5 g/s*. The inset image of Figure 2 shows the micro-hybrid thruster firing during a 1-second pulse from one of the initial demonstration tests.

In the prototype unit the ABS segment was contained within a polycarbonate shell to capture and direct the vaporized fuel material. The oxidizer flow path of Figure 2 is from left to right, and the current flow is from right to left. The high voltage electrode is attached to the downstream side of the *ABS* grain segment and drops to ground on the upstream end.

Originally the unit was tested using a commercially procured "stun gun," but was eventually replaced by a precision high-voltage power supply.[57] The power supply has a selectable current-limit up to 13 mA, and is capable of delivering a maximum of 130 watts at *10,000 VDC*. During the proof-of-concept tests, ignition was achieved with as little as 8-Watts power input at approximately *1000 VDC*.

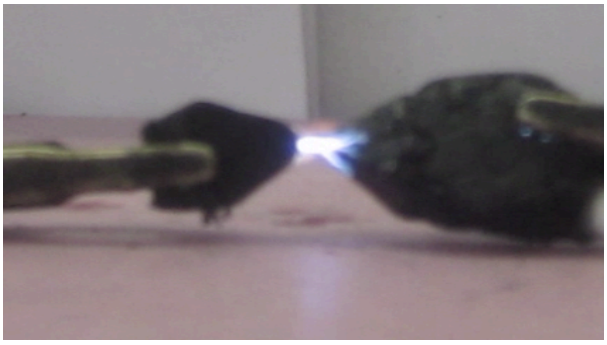

Figure 1. Electrostatic Spark Across Two ABS Test Segments.

The 2.5 cm diameter hydrocarbon-seeding grain for this prototype unit was fabricated using a Stratasys Dimension® 3-D Fused Deposition Model (*FDM*) printer. Figure 3 shows a seeding fuel grain segment during evaluation testing. Here the low-amperage current enters the high-tension lead, and then conducts along the surface of the *ABS* segment before jumping the gap to produce the high-voltage spark. The electrostatic spark and vaporized fuel material are clearly visible.

The grain segments used for this prototype unit started with typical electrical impedances exceeding 1 *MΩ*. Input impedances dropped to less than *10 kΩ* after multiple ignitions. The progressive drop in impedance eventually rendered the grain segment unusable. Fortunately, the "micro-hybrid" prototype was pulse-fired for up to 27 consecutive burns on a single ABS grain segment.

To date no optimization study has been performed to identify the best grain geometry for electrolytic ignition. Fortunately, because the grain segments are fabricated using rapid-prototyping technology,

changing the grain geometry is as simple as modifying the 3-D printer CAD-file.

Hydrocarbon-Seeded Ignitor Demonstration Tests

The proof-of-concept prototype depicted in Figure 2 was adapted and tested as a non-pyrotechnic, multi-use, multipurpose ignitor. In a series of demonstration tests the "micro-hybrid" prototype unit was used to successfully ignite a 98-mm diameter, 800-N thrust, hybrid rocket motor multiple consecutive times without hardware changeover or propellant replenishment. These tests used a well-known motor configuration that had been previously tested and characterized using pyrotechnic ignitors before inserting the micro-hybrid ignitor as a "drop-in" replacement. The 98-mm hybrid motor was adapted from a commercially available Cesaroni® solid-rocket 98-mm motor case by replacing the original ejection charge on the motor cap with a single port oxidizer injector and two ignitor ports. The hybrid motor uses N_2O as the oxidizer and main hybrid fuel grains were composed of either *ABS* or *HTPB*.

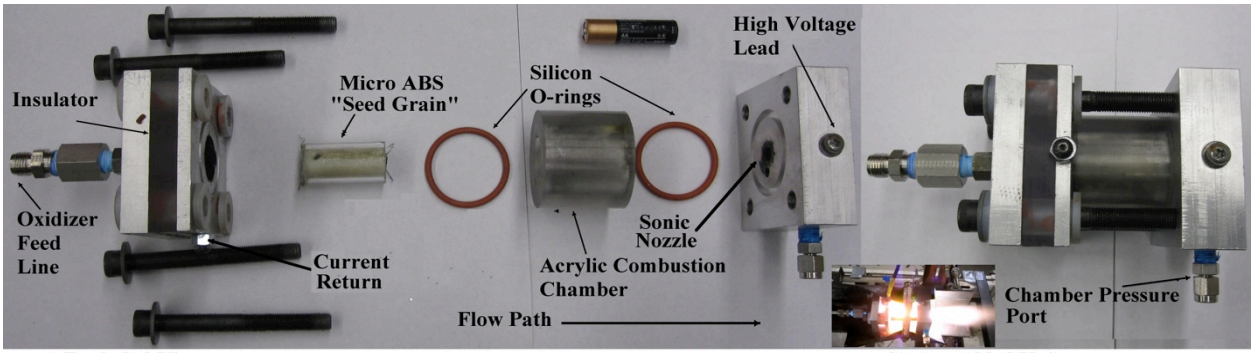

Figure 2. "Hydrocarbon Seeded" Micro-hybrid Thruster Prototype.

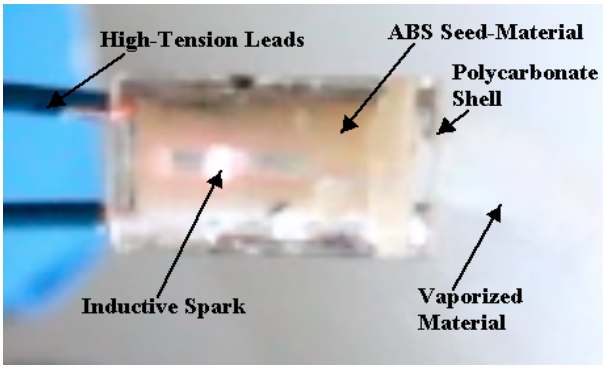

Figure 3. Developmental Ignitor Grain Segment During Early Evaluation Testing.

Figure 4 shows an exploded view of the micro-hybrid ignitor interface to the 98-mm motor injector cap. The hydrocarbon-seeded ignitor replaces one of the single-use solid-propellant (pyrotechnic) ignitors formerly used to ignite the 98-mm hybrid motor. The other ignitor port was plugged and unused for these demonstration tests. Figure 5 shows the prototype ignitor with a 1.25 cm diameter ABS seeding grain, interfaced to the motor cap, and firing during evaluation tests.

Figure 6 shows a functional diagram of the test setup used for the 98-mm motor ignition tests The ignition system for this demonstration experiment was extremely simple, consisting of an oxidizer supply, flow regulator, run valve, back flow valve, power supply, trigger relay, and the ignitor assembly. The motor cap was wired to the high voltage return and very strongly to ground) so that the entire voltage drop occurs across the *ABS* seed-grain spark gap -- between the high voltage pass-through in the ceramic insulator and the high voltage return. As a safety measure, to prevent backflow from the main motor into the ignitor chamber, the ignitor oxidizer feed pressure was regulated at approximately 700 kPa (100 psi) higher than nominal chamber pressure. A backflow check-valve was also installed in the ignitor oxidizer feed line in case of higher than expected chamber pressure occurred in the 98 mm motor.

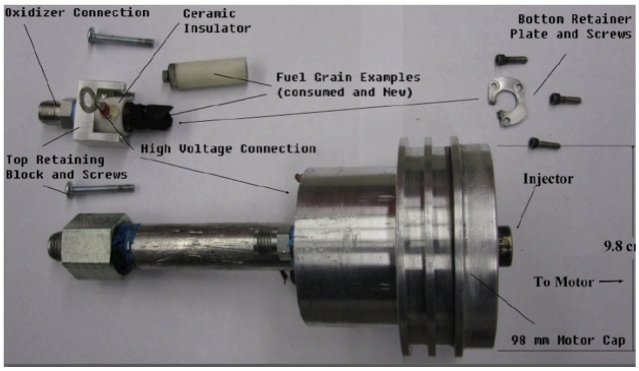

Figure 4. Ignitor Interface to 98-mm Hybrid Motor Injector Cap

A National-Instruments Compact-DAQ® 9417 automation controller with a 4-slot backplane with multiple analog input (AI), analog output (AO), Digital output (DO), and Thermocouple (TC) modules managed all process controls including run tank filling, motor firing sequences, fault diagnostics, situational awareness displays, emergency options, and test data logging. Process automation was essential for

Figure 5. Ignitor Evaluation Tests

establishing timing consistency of the hydrocarbon seeding ignition process.

Figure 7 plots typical results from 6 successive ignition tests. In order to avoid any issues associated with a potential "hard start," the igniter GOX flow valve was opened 500 ms after electrical power was delivered to the ignitor fuel grain. For the 98 mm motor ignition tests, the ignitor burn was preset to terminate 375 ms after the main oxidizer valve was opened. The main motor oxidizer flow continued for 2.25 seconds after the ignitor flow was terminated. The igniter burn time overlapped main motor ignition by approximately 100-200 ms. Combustion latencies from oxidizer valve opening to full ignition were timed to be less than 10 msec.

The mean ignitor output mass flow rate was approximately *3.7 g/s,* and this value is compared with the main motor N_2O flow rate of approximately *350 g/s.* The required power input to the ignitor started at less than 10 Watts for the initial burn, and dropped to 2 Watts for the final burn. The total burn input energy averaged less than 5 joules. The gas byproducts from the hydrocarbon-seeding process exceeded 2400 C with a mean output enthalpy rate of nearly 30 kW -- *an output-to-input power ratio of more than three orders of magnitude!* The mean total output energy for each igniter burns exceeded 25 kJ.

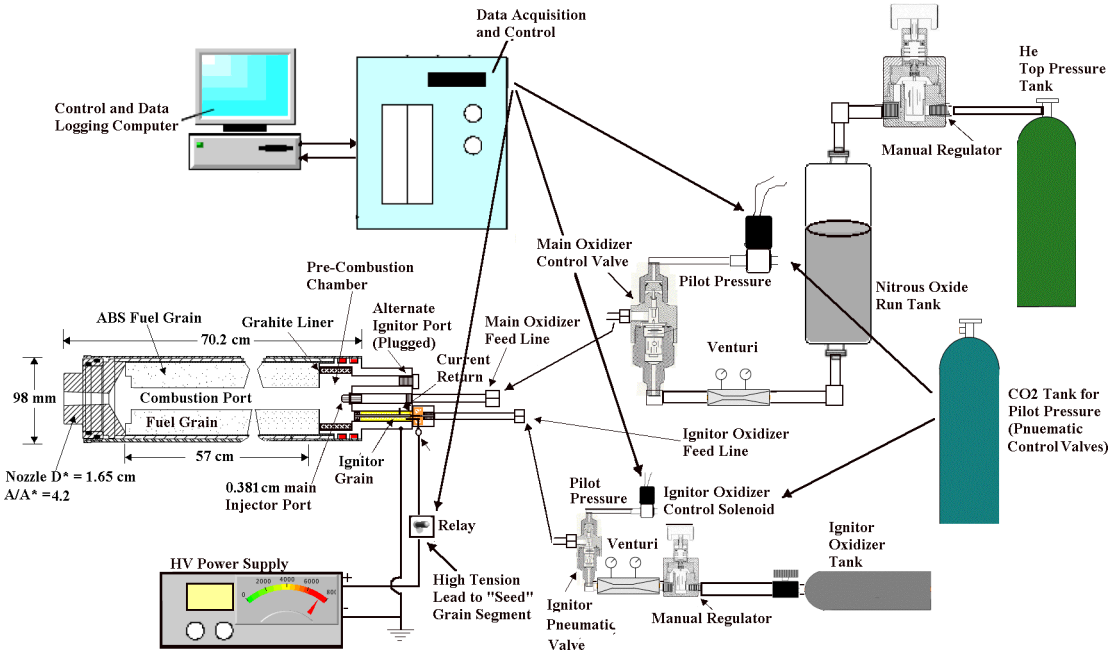

Figure 6. Schematic of Apparatus Used for Prototype 98 MM Hybrid Motor Ignition Tests.

Nitrous oxide-based hybrid motors require significant ignition energy and typically require multiple, staged, solid-propellant charges to initiate combustion. This series of tests marks the first time that a hybrid motor has been electrostatically ignited using a low-wattage input and a non-pyrotechnic, reusable ignitor. The ignition process works seamlessly with the only limit to the number of available repeat firings being the amount of ABS seed material that can be fit into the injector cap. This approach to motor ignition also makes the system highly resistant to potential issues with Hazards of Electromagnetic Radiation to Ordnance (Ref. 35).

Because the small ABS fuel segments used to "seed" the ignitor flow can be quickly and inexpensively fabricated using FDM rapid-prototyping machines, this process stands in contrast to catalytic ignition systems that are "one-off" fabricated using expensive noble metals and supporting substrates. The electrostatic source used to initiate the combustion process can be provided inductively, and uses only a few joules per ignition. *The 5 J ignition energy is compared to the typical 15 kJ preheat energy required by the ECAPS Prisma thruster. (Ref. 39)* Thus this non-pyrotechnic ignition demonstration is a significant step along the way towards developing a reliable non-catalytic ignition system for *IL*-based propellants.

NUMERICAL MODEL OF THE HYDROCARBON-SEEDED IGNITION PROCESS FOR IL-BASED PROPELLANTS

Although HAN-based propellants are slightly lower performing than ADN-based propellants, HAN/water solutions can be procured for as little at $140 per $^1/_2$ liter, and the solution is readily availability from a variety of commercial vendors. Thus, as a cost saving measure, binary HAN-water solutions will be used for this project. HAN is an inorganic compound with the chemical formula NH_3OHNO_3.[59,60] HAN exhibits strong ion-ion interactions where $[NH^3OH]^+$ is the cation and $[NO_3]^-$ acts as the anion. HAN is highly soluble in water, has a molecular weight of *96.04 kg/kg-mol,* and has an effective room temperature density of *1809.48 g/l*. This choice of "green" oxidizer fits well with NASA's commitment to the AF-M315E propellant for the "Green Propellant" TDM flight test. (Ref. 11)

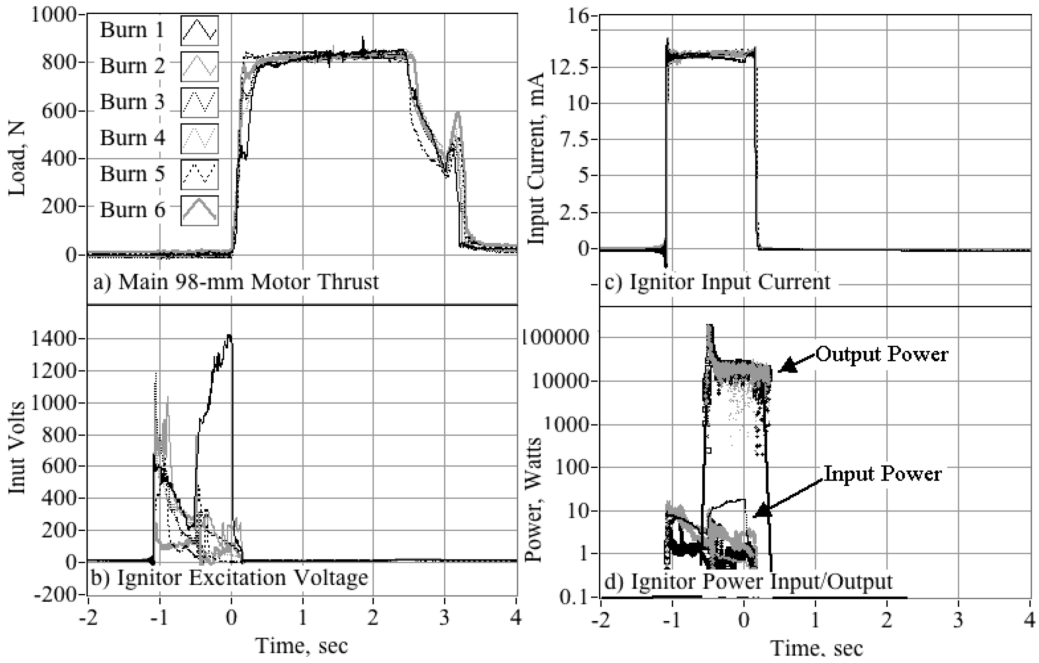

Figure 7. Typical Ignition Tests Results for Micro-Hybrid Ignitor Prototype.

As mentioned previously, Courthéoux, et al. (Ref. 41) demonstrated that up to 387 W/g/s of heating input rate was required to initiate thermal dissociation of a 60% binary HAN-water solution once all of the water in solution had vaporized. As shown in Figure 7, the proof-of-concept ignition tests demonstrate an output capability of approximately 30 kW at a mass flow rate of approximately 4 g/s. Thus the micro-hybrid ignitor design is at least capable of producing 7500 W/g/s of heating rate output and there exists considerable promise for adapting this concept for binary *HAN/H_2O* and ternary *HAN/H_2O/fuel* mixtures.

This section developments the analytical model used to guide the ignitor design and its integration onto a proof-of-concept HAN-based thruster. The model assumes non-catalytic thermal ignition using a modified version of the micro-hybrid ignitor as previously presented. The simulation architecture assumes a single "micro-hybrid" ignitor, with one or more propellant injectors. For this model a binary *HAN/H_2O* propellant solution is assumed.

All equations used to describe the fluid mechanics assume quasi-1 dimensional flow. Vander Waals equations are used to model the two-phase flow properties of the water component of the HAN-solution. The standard de Laval nozzle flow equations are used to perform choking mass flow and thrust calculations.

Ignitor Flow Model

The micro-hybrid ignitor mass flow model assumes a prescribed chamber pressure P_{ign}, combustion efficiency η^*, and oxidizer -to-fuel (*O/F*) ratio. The flow model checks to identify when the ignitor exit port is choked. When the ratio of the ignitor pressure to the main combustor pressure P_c, exceeds the critical value

$$\frac{P_{ign}}{P_c} > \left(\frac{\gamma_{ign}+1}{2}\right)^{\frac{\gamma_{ign}}{\gamma_{ign}-1}}, \quad (1)$$

the exit is choked, and the exit mass flow is calculated by the deLaval choking mass flow equation

$$\dot{m}_{ignitor} = C_{d_{ign}} \cdot A^*_{ign} \cdot \sqrt{\frac{\gamma_{ign}}{R_g} \cdot \left(\frac{2}{\gamma_{ign}+1}\right)^{\frac{\gamma_{ign}+1}{\gamma_{ign}-1}}} \cdot \frac{P_{ign}}{\sqrt{T_{ign}}} \quad (2)$$

When, the pressure ratio is less than the critical value, the non-choked isentropic flow formula is used,

$$\dot{m}_{ignitor} = C_{d_{ign}} \cdot A^*_{ign} \cdot P_{ign} \times \sqrt{\frac{1}{R_{g_{ign}} \cdot T_{ign}} \left(\frac{2 \cdot \gamma_{ign}}{\gamma_{ign}-1}\right) \cdot \left[\left(\frac{P_{ign}}{P_c}\right)^{\frac{2}{\gamma_{ign}}} - \left(\frac{P_{ign}}{P_c}\right)^{\frac{\gamma_{ign}+1}{\gamma_{ign}}}\right]} \quad (3)$$

In Eqs. (2) and (3) the exhaust gas temperature is calculated as

$$T_{ign} = \left(\eta^*\right)^2 \cdot T_{flame} \quad (4)$$

where η is the combustion efficiency of the ignitor. Also, in Eq. (3) A^*_{ign} represents the physical exit area of the ignitor and not the equivalent choking flow area. The ignitor discharge coefficient $C_{d\ ign}$ is allowed as a placeholder, and for all but very small exit diameters can be assumed as unity. The ignitor exhaust gas specific enthalpy is calculated assuming a calorically perfect gas

$$h_{ign} = C_{p_{ign}} \cdot T_{ign} \quad (5)$$

The rate at which total enthalpy exits the ignitor is

$$\dot{H}_{ign} = \dot{m}_{ignitor} \cdot C_{p_{ign}} \cdot T_{ign} \quad 6)$$

shows the the variation of the exhaust product ideal flame temperature T_{flame}, ratio of specific heats γ, molecular weight M_w, and gas-specific constant R_g, as a function *O/F* ratio and P_{ign}. The plotted values were calculated using the industry standard NASA equilibrium chemistry code "Chemical Equilibrium with Applications (CEA).[61] These calculations assume frozen chemistry at the choke point. The ignitor design leverages the hybrid fuel regression and chamber pressure model developed by Eilers and Whitmore.[62]

HAN Solution Injector Flow Model

The HAN solution injector model assumes incompressible flow, and the standard incompressible injector mass flow model is used

$$\dot{m}_{\substack{HAN/\\H_2O}} = \left(C_d A_{inj}\right)_{\substack{HAN/\\H_2O}} \sqrt{2 \cdot \rho_{\substack{HAN\\H_2O}} \cdot \left(p_{inj} - p_c\right)} \quad (7)$$

In Eq. (7) the first term on the right had side of the equation is the total discharge area of the HAN-water solution injector, $\rho_{HAN/H2O}$ is the density of the injected HAN solution, and P_{inj} is the HAN solution feed pressure. The solution thermodynamic and transport properties are dependent on the HAN mass-concentration.

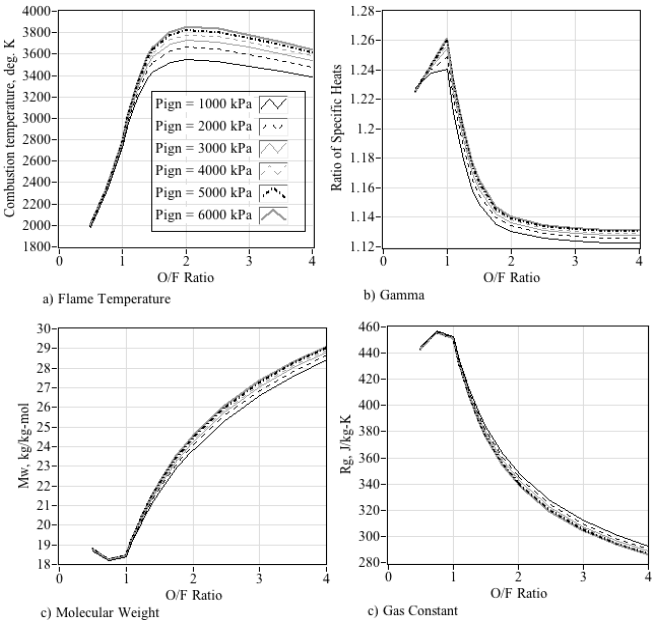

Figure 8. Exhaust Properties for GOX/ABS Combustion.

There is no general consensus on the specific heat of *HAN/H2O* solutions of varying concentration. Schoppelrei, et al[63] measured the specific heat of a 24% aqueous HAN solution at 4300 J/kg-K. This data is curve-fit for solutions with concentrations varying from 0 to 100% using the mole-fraction formula,

$$C_{p_{HAN/H_2O}} = \frac{\frac{M_{HAN}}{M_{total}} \cdot M_{w_{HAN}} \cdot C_{p_{HAN}} + \frac{M_{H_2O}}{M_{total}} \cdot M_{w_{H_2O}} \cdot C_{p_{H_2O}}}{M_{w_{HAN/H_2O}}} \quad (8)$$

and Figure 10 plots this result as a function of HAN-mass concentration. The specific enthalpy of the injected HAN-solution is calculated using the calorically perfect fluid assumption and the rate at which total solution enthalpy is injected into the combustion chamber is

$$\dot{H}_{HAN/H_2O} = \dot{m}_{HAN/H_2O} \cdot C_{p_{HAN/H_2O}} \cdot T_{HAN/H_2O} \quad (9)$$

where $T_{HAN/H2O}$ is the temperature of the injected solution, and the specific is calculated using Eq. (14).

The presence of the HAN ions in solution has the effect of raising the solution boiling point above the normal boiling point of pure water. The Clausius-Clapeyron equation[64] is used to calculate this elevated boiling point. For water in the saturated state, the enthalpy of vaporization is also strongly a function of temperature.[65] Figure 11 plots the enthalpy of vaporization for water as a function of temperature, the nominal boiling point as a function of pressure, and the calculated boiling point for the HAN/water solution as a

function of mass fraction. Figure 11a also plots the equivalent molar concentration of HAN is a 1-liter volume of solution (M).

Combustion Chamber Mass Balance

The combustor mass-balance assumes a homogeneous vapor model. That is, the incoming *HAN/H_2O* solution is sufficiently atomized by the injector that it behaves as a vapor. Real-gas properties are accounted for using Van der Waals Equation. The accumulated mass in the combustion chamber is calculated by

$$\frac{d}{dt}\left(m_c\right) = \dot{m}_{ignitor} + \dot{m}_{HAN/H_2O} - \dot{m}_{exit} \quad . \qquad (11)$$

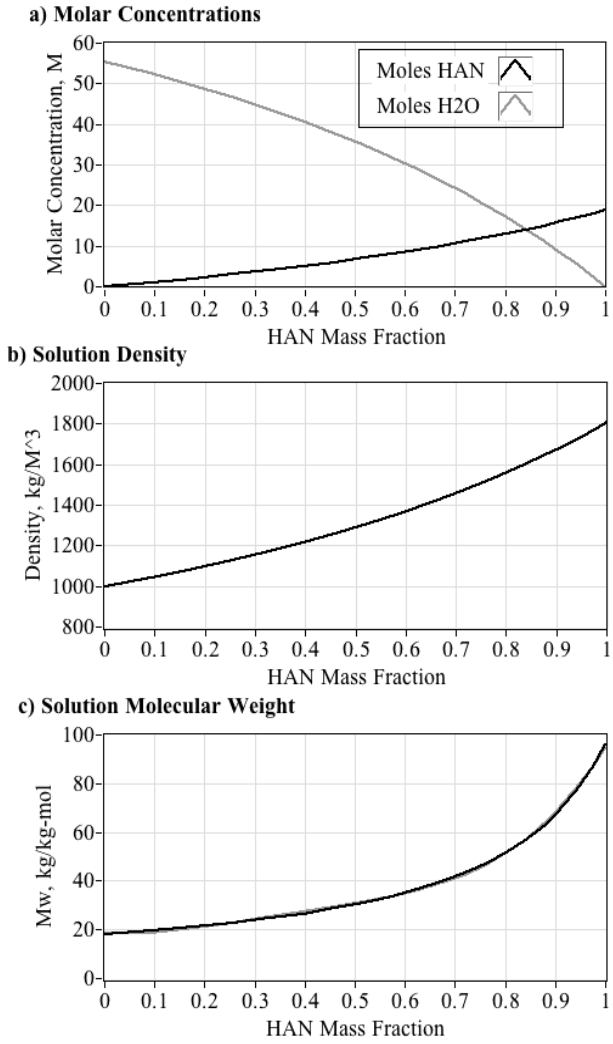

Figure 9. HAN/H_2O Solution Molar Concentrations, Molecular Weight, and Density.

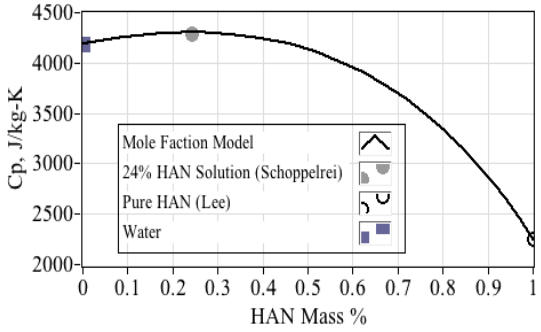

Figure 10. Calculated Specific Heat for HAN/H_2O Solution with Varying Mass Concentration.

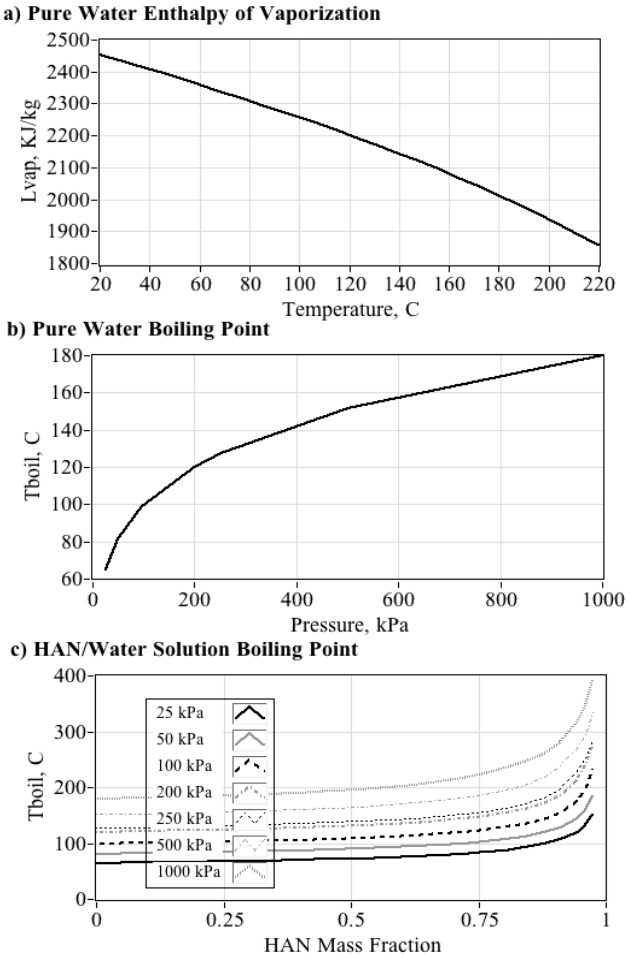

Figure 11. Enthalpy of Vaporization, Boiling Point of Pure Water, and Boiling Point of HAN-Water Solution.

Eqs. (2) and (3) are used to calculate the ignitor mass flow and Eq. (7) is used to calculate the HAN/H_2O injector mass flow. The nozzle exit mass flow is calculated using the one-dimensional flow models for compressible flow.

The thermodynamic properties of the collected gases in the chamber are calculated based on the accumulated mole fractions in the combustion chamber. Eq. (11) is integrated to calculate the total mass that has

accumulated in the chamber. The relative compositions of *HAN/H₂O* solution and ignitor by-products are calculated by assuming that the respective exit mass flow are proportional to inlet mass flows of each propellant. The chamber vapor mixture is assumed to be homogeneous with no change in species due to chemical reactions.

The two-phase properties of the water and HAN components of the injected solution are approximated using Van der Waals equation of state,[66]

$$p = \left[\frac{1}{1 - b \cdot \frac{\rho}{M_W}} - a \cdot \frac{\frac{\rho}{M_W}}{R_u T} \right] \cdot \rho R_g T \quad . \quad (12)$$

The bracketed term in Eq. (12) is referred to as the fluid *compressibility factor*. lists the critical temperature, critical pressure and the Van der Waals parameters {*a, b*} for *HAN*[67] and *H₂O (Ref 66).* The units of *a* are *kPa-m⁶/kg-mol²*. The units of *b* are *m³/kg-mol.*

Table 1: Van der Waals Model Parameters for HAN/H₂O

Parameter	T_{crit} *(K)*	P_{crit} *(kPa)*		*b*
HAN	*763.00*	*7700.7*	*2204.96*	*0.102984*
H₂O	*647.10*	*22,058.5*	*553.62*	*0.030489*

Within each time frame, after the accumulated masses and mole fractions of collected the propellants in the chamber are calculated, the individual propellant densities are calculated by dividing the accumulated propellant masses by the chamber volume, V_c,

$$\rho_{HAN} = \frac{m_{HAN}}{V_c}, \; \rho_{H_2O} = \frac{m_{H_2O}}{V_c}, \; \rho_{ign} = \frac{m_{ign}}{V_c} \quad , \quad (13)$$

The Van der Waals model is used to calculate the partial pressures for *HAN* and *H₂O*, and the ideal gas law is used to calculate the partial pressure for the ignitor combustion products. The total chamber pressure is calculated using the mole-fractions of each propellant component.

$$P_c = \frac{P_{pHAN} \cdot M_{HAN} + P_{pH_2O} \cdot M_{H_2O} + p_{p\,ign} \cdot M_{ign}}{M_{HAN} + M_{H_2O} + M_{ign}} \quad . \quad (14)$$

Combustion Chamber Enthalpy Balance

The chamber enthalpy balance treats the entire chamber as a lumped mass with no heat loss to the chamber walls, and assuming a calorically perfect fluid. When this energy balance is performed the rate of enthalpy change within the combustion chamber is

$$\dot{H}_c = \dot{m}_{\substack{HAN \\ H_2O}} \cdot \left(C_{p\,\substack{HAN \\ H_2O}} \cdot T_{\substack{HAN \\ H_2O}} - L_{\substack{vap \\ H_2O}} \cdot (1 - f) + \dot{m}_{\substack{HAN \\ H_2O}} \cdot \Delta q_{\substack{HAN \\ H_2O}} \right) + \dot{m}_{ign} \cdot C_{Pign} \cdot T_{ign} - \dot{m}_{exit} \cdot C_{p_c} \cdot T_c \quad . \quad (15)$$

In eq. (15) L_{vap/H_2O} is the latent heat of vaporization of the water in the solution, *f* is the HAN mass fraction, and $\Delta q_{HAN/H_2O}$ is the energy density of the solution at the given HAN-mass concentration minus the decomposition energy barrier of 387 J/g. (Ref. 41) Figure 12 plots the solution energy density as a function of HAN mass concentration.[69] The combustion chamber temperature is calculated using calorically perfect fluid assumptions,

$$T_c = \frac{H_c}{C_{P_c} \cdot \left(m_{\substack{HAN \\ H_2O}} + m_{ignitor} \right)} \quad . \quad (16)$$

The enthalpy of evaporation term in Eq. (15) is active only when the combustion chamber temperature exceeds the vaporization point of the solution as calculated plotted in Figure 11.

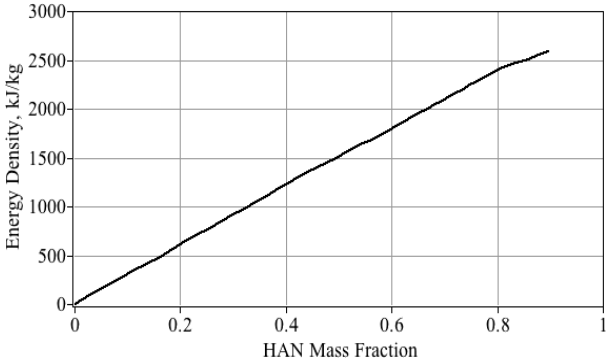

Figure 12. HAN/Water Solution Energy Density as a Function of HAN Mass Concentration.

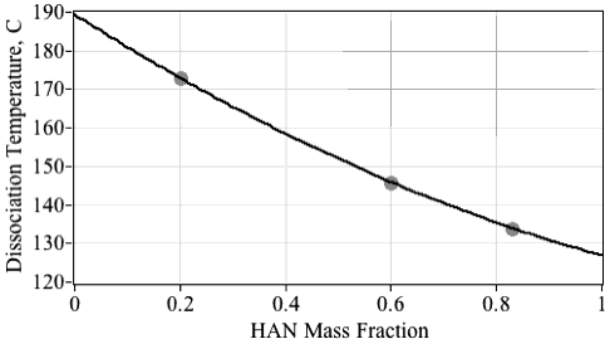

Figure 13. HAN/Water Solution Thermal Decomposition Temperature.

As mentioned previously, Courthéoux et al. (Ref. 41) investigated the thermal decomposition points for HAN/H₂O solutions with 20%, 60%, and 83% HAN mass concentrations. Figure 13 plots this decomposition curve with data extrapolated from 0 to 100% HAN concentration. The HAN energy input to the combustion equation, Eq. (15), is active in only when the combustor temperature exceeds the thermal decomposition temperature of Fig. 13.

HAN Solution Decomposition Rates

Multiple researchers including 1) Lee and Litzinger,[70] 2) Pan et al,[71] 3) Vosen,[72] 4) Kondrikov et

al.,[73] and 5) Katsumi and Hori[74] have studied the decomposition rates for aqueous HAN-solutions and HAN-based propellant solutions. There is considerable disagreement amongst the published results; however, there exists a general consensus that high pressures exhibit a suppressing effect on the HAN solution decomposition rates for pressures above 10 MPa.

The measurements taken by Katsumi and Hori are most applicable to the chamber pressure levels to be expected for SmallSat-propulsion systems. Katsumi and Hori prepared HAN/water solutions varying in concentration from 50% to 85% and burned the binary mixtures in a constant-pressure strand burner purged with nitrogen gas. Combustion pressures were varied from 1-10 MPa. At these lowered pressure levels Katsumi and Hori showed that there was a strong positive influence of chamber pressure on the linear burning rate.

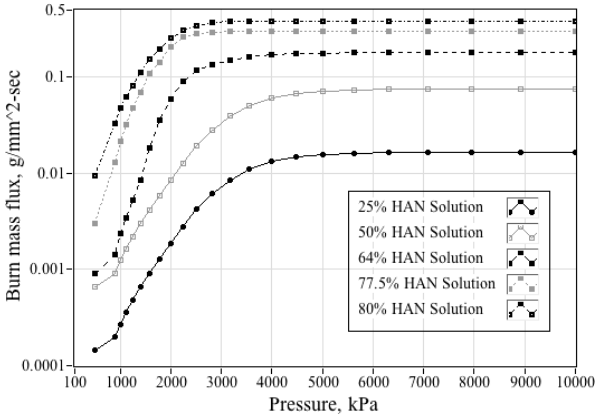

Figure 14. HAN Solution Mass Flux as Function of Pressure and HAN Mass Concentration.

Multiplying the linear burn rate curves presented by Katsumi and Hori by the corresponding solution density (taken from Figure 9) approximates the decomposition mass-flux as a function of HAN concentration and chamber pressure. Figure 14 plots the resulting mass flux model with data extrapolated to 25% HAN concentration, and 500 kPa chamber pressure. In this model the mass flux curves drop steeply when the combustion pressure drops below 2000 kPa. Below 1000 kPa operating pressure there is little available kinetic-rate data available; thus, it is desirable to design the system to achieve a steady-state burn pressure above 1000 kPa at a minimum to reduce the operating uncertainty and ensure adequate HAN decomposition efficiency.

Required Chamber Dwell-Time

In order to achieve reasonable combustion efficiency, the combustion chamber must be sufficiently large so that the propellant solution "dwell time" allows for all of water to be evaporated from the injected solution; also allowing for the remaining liquid HAN to decompose. A key element in this calculation is the drop atomization size. For this droplet size calculation the mean droplet distribution model developed by Hinze is used.[75] This model correlates the droplet size to the specific mechanical power of the injected fluid spray. Assuming a conventional log-normal drop size distribution function,[76] the mean droplet size can be expressed as

$$D_{droplet} = 0.23 \cdot \left(\frac{\sigma^3{}_{HAN/H_2O}}{\rho_c} \cdot \left(\frac{V_c \cdot \rho_{HAN/H_2O}}{P_{inj} \cdot \dot{m}_{HAN/H_2O}} \right)^2 \right)^{1/5} \quad . \quad (17)$$

In Eq. (18) ρ_c is the mean density of the vaporized propellants within the chamber, P_{inj} is the injector feed pressure, and σ_{inj} is the surface tension of the injected HAN-water solution. For this calculation, the fluid tension of water is assumed, 0*.073 N/m* at 290 K.

The mean droplet size calculated by Eq. (17) is used to calculate the water-content evaporation time for the atomized solution. The rate of evaporation of the water is modeled by Langmuir's equation for free evaporation,[77]

$$\left(\dot{m}_{H_2O}\right)_{vaporized} = A_{surf} \left(P_{vapor} - P_{p_{H_2O}} \right) \cdot \sqrt{\frac{1}{2\pi \cdot \left(R_g\right)_{\substack{H_2O \\ vapor}} T_c}} \quad . \quad (18)$$

In Eq. (18) P_{vapor} is the vapor pressure of water at the combustion chamber temperature, as calculated using Eq. (20), T_c is the chamber gas temperature in absolute units, and A_{surf} is the collected surface area of evaporation. The partial pressure of water vapor in the chamber is calculated using Eqs. (13)-(15). The gas constant in Eq. (18) is based on the molecular weight of water and not the molecular weight of the HAN-water solution. The mass of water contained in each droplet is

$$m_{\substack{H_2O \\ droplet}} = \left(1 - f\right) \cdot \rho_{\substack{HAN/ \\ H_2O}} \cdot \frac{\pi}{6} \cdot D^3{}_{droplet} \quad . \quad (19)$$

In Eq. (19) f is the HAN solution mass concentration. The time required for the water in each droplet to vaporize is directly proportional to the droplet atomization size, and is approximated by Eq. (20). The mass of HAN contained within each propellant drop is given by Eq. (21), and the required HAN decomposition time is given by Eq. (22). In Eq. (22) B_{flux} is the HAN decomposition mass flux derived from the data presented by Figure 14. Eqs. (20)-(22) are presented on the following page.

Required Chamber Length

As mentioned in the introduction to this section, the chamber geometry must be large enough to allow sufficient dwell time for all of the water to be evaporated from the injected solution, and also allow for the remaining liquid HAN to dissociate. Conservatively, the dwell time requirement is calculated as the sum of the water evaporation time and the HAN decomposition time, Eq. (13).

$$\Delta\tau_{\substack{H_2O \\ vapor}} = \frac{m_{droplet}}{\left(\dot{m}_{H_2O}\right)_{vaporized}} = \frac{\left(1-f\right)\cdot\rho_{\substack{HAN/ \\ H_2O}}\cdot\frac{\pi}{6}\cdot D^3{}_{droplet}}{\pi\cdot D^2{}_{droplet}\left(P_{vapor}-P_{p_{H_2O}}\right)\cdot\sqrt{\frac{1}{2\pi\cdot\left(R_g\right)_{\substack{H_2O \\ vapor}}T_c}}} =$$

$$\sqrt{\frac{\pi}{18}\cdot\left(R_g\right)_{\substack{H_2O \\ vapor}}T_c}\,\frac{\left(1-f\right)\cdot\rho_{\substack{HAN/ \\ H_2O}}\cdot D_{droplet}}{\left(P_{vapor}-P_{p_{H_2O}}\right)\cdot} \quad . \tag{20}$$

$$m_{\substack{HAN \\ droplet}} = f\cdot\rho_{\substack{HAN/ \\ H_2O}}\cdot\frac{\pi}{6}\cdot D^3{}_{droplet} \quad . \tag{21}$$

$$\Delta\tau_{dwell} = \Delta\tau_{\substack{H_2O \\ apor}} + \Delta\tau_{\substack{HAN \\ dissociation}} \quad . \tag{23}$$

Assuming a combustion "efficiency factor," where $0 < \eta_{eff} < 1$, the required chamber length along the direction of flow is calculated as

$$L_{chamber} = \frac{\Delta\tau_{dwell}\cdot V_{inj}}{\eta_{eff}} \quad . \tag{24}$$

The *HAN/H₂O* solution injection velocity is approximated by

$$L_{chamber} = \frac{\Delta\tau_{dwell}\cdot V_{inj}}{\eta_{eff}} = \frac{C_{d_{HAN/H_2O}}\cdot\cos\left(\theta_{inj}\right)}{\eta_{eff}}\cdot\sqrt{2\cdot\left(\frac{P_{HAN/H_2O}-P_c}{\rho_{HAN/H_2O}}\right)} \quad . \tag{25}$$

In Eq. (25) θ_{inj} is the injection angle of the *HAN/H₂O* solution relative to the longitudinal axis of the combustion chamber.

HAN-Solution to Jgnitor Mass flow Ratio

To ensure that the ignitor will provide sufficient enthalpy to assure efficient decomposition in the HAN-solution, there exist a maximum allowable HAN-solution to Ignitor output mass flow ratio. Equation (26) presents this calculation,

$$\frac{\dot{m}_{\substack{HAN/ \\ H_2O}}}{\dot{m}_{ignitor}} = \frac{c_{p_{ignitor}}\cdot T_{0_{ignitor}}\cdot\eta^2{}_{ignitor}}{\left(1-f\right)\cdot\left(c_{p_{H_2O\,Liquid}}\cdot\left(T_{boil}-T_{initial}\right)+L_{H_2O}\right)+f\cdot\left(\Delta H_{\substack{HAN/barrier \\ H_2O}}\right)} \quad . \tag{26}$$

The numerator of the energy balance term on the right hand side of Eq. (26) represents the specific power output of the ignitor, and the terms in the denominator represent the specific energy required to heat the HAN-solution to the boiling point, vaporize the water in solution, and overcome the HAN dissociation energy barrier, 387 J/kg. Conservatively, this calculation assumes no heat contribution from partial dissociation of the HAN in solution.

$$\Delta\tau_{\substack{HAN \\ dissociation}} = \frac{m_{\substack{HAN \\ droplet}}}{\left(\dot{m}_{HAN}\right)_{dissociation}} = \frac{\frac{f}{6}\cdot\rho_{\substack{HAN/ \\ H_2O}}\cdot\pi\cdot D^3{}_{droplet}}{\pi\cdot D^2{}_{droplet}\cdot B_{flux}} = \frac{1}{6}\left(\frac{f\cdot\rho_{\substack{HAN/ \\ H_2O}}\cdot D_{droplet}}{B_{flux}}\right) \quad . \tag{22}$$

DEVELOPMENTAL THRUSTER GEOMETRY AND TEST APPARATUS

The model presented in the previous section was used to design a prototype thruster of a size that is useful for SmallSat propulsion applications, but still sufficiently large to allow fabrication using the conventional manufacturing techniques available at Utah State University. Figure 15 presents a schematic of the lab-weight developmental thruster. The developmental thruster is approximately *22 cm (8.6 in)* long and *6.35 cm (2.5 in)* wide. The internal volume of the combustion chamber is approximately 225 cm^3. Eqs. (12)-(15) are used to adjust the chamber design parameters to ensure an operating chamber pressure between *1000 kPa (145 psia)* and *2000 kPa (290 psia)*. This chamber pressure range is calculated to produce a thrust level between 12.5 N (2.8 lbf) and 25 N (5.6 lbf).

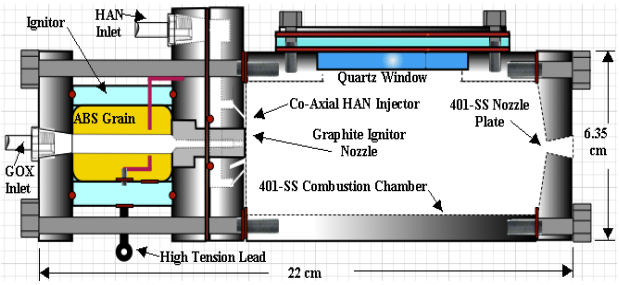

Figure 15. Developmental Thruster Design.

The injector plate and combustion chamber are fabricated from 400-series stainless steel for ensured compatibility with HAN.[78] A quartz window allows high-speed video capture of the injection, mixing, and combustion processes. The coaxial impinging injector will considerably improve the atomization of the injected propellant and enhances the ignitability of the HAN-solution. The impinging 45° flow stream should also accelerate the HAN-decomposition time. The

igniter bolts to the top of the HAN injector plate, and the high voltage electrical lead runs to the ABS fuel grain through a non-conductive polycarbonate pressure sleeve. The entire unit is grounded and provides the return path for the high-tension lead.

The design oxidizer-to-fuel (*O/F*) ratio for the igniter is approximately 4.0, and is significantly higher than optimal for *GOX/ABS* (O/F_{opt}=*1.5)*. This *O/F* ratio was chosen to maximize the number of ignitions available for a single igniter fuel grain.

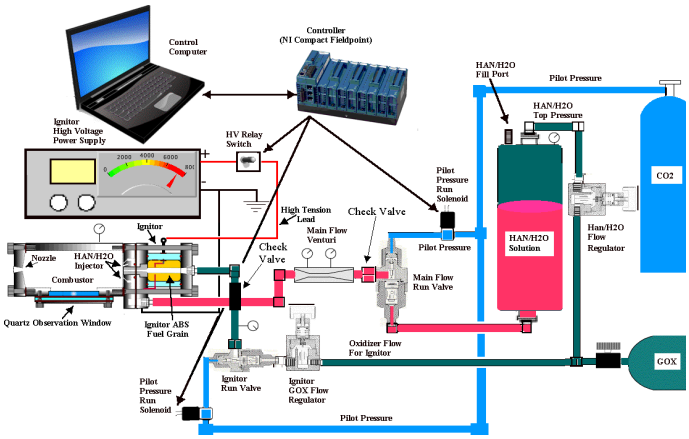

Figure 16. Experimental Apparatus for HAN-thruster Development Tests.

Figure 16 shows the piping and instrumentation diagram (P&ID) of the experimental apparatus used perform early stage system development tests. Here a single gaseous oxygen (GOX) source is used both as the igniter oxidizer and as the top-pressurant for the HAN solution. Each feed pressure is independently regulated. The oxidizer feed pressure is maintained at approximately a factor of 1.25 higher than expected nominal chamber pressure to ensure that injector feed-coupling does not occur. The injector feed pressure is adjustable to ensure sufficient enthalpy for reliable propellant ignition.

EXAMPLE MASS FLOW RATIO, COMBUSTION TEMPERATURE, AND CHAMBER PRESSURE, SIZE CALCULATIONS

As calculated using Eq. 26, Figure 17 plots maximum allowable *HAN-solution-to-Ignitor* mass flow ratio as a function of the solution concentration. At low solution concentrations, a large quantity of water must be vaporized before dissociation of the nearly pure liquid-HAN can occur. Thus, a significantly lower-solution-to-ignitor mass flow ratio is allowable, i.e. a higher total ignitor output enthalpy is required for a given HAN solution mass flow. As the solution concentration drops, ta smaller ignitor mass flow is allowable. At 60% HAN-concentration the Solution-to-ignitor mass flow ratio is approximately 3:1. This value was chosen as the design point for the developmental thruster. As required, the ignitor output mass flow will be increased by increasing the GOX feed pressure.

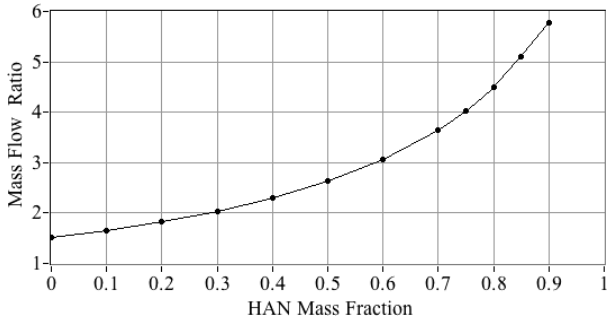

Figure 17. Allowable HAN-Solution to Ignitor Mass flow Ratio.

Figure 18 summarizes the results of the modeling calculations for the 25-N thruster operating 2000 kPa chamber pressure. These calculations assume 90% HAN-decomposition efficiency. Figure 18(a) plots the maximum and sustained temperatures as a function of HAN concentration. Figure 18(a) also plots the dissociation temperature for the HAN solution; these data are taken from Figure 13.

Below 25% solution concentration the ignitor provides insufficient power output to allow the thruster to reach decomposition temperature. For solution concentrations from 25% to approximately 60%, the ignitor provides sufficient energy to initiate HAN-decomposition; however, the decomposition provides insufficient power to overcome the latent heat of the water in solution. The chamber remains near the boiling point of the solution. Only once the solution density is above 60% does the energy from decomposition exceed the latent heat of the water in solution, and the chamber temperature climbs above the solution boiling point. Above 70% HAN-concentration there is a large jump in the chamber temperature. For the lower concentration solutions, the maximum temperatures occur immediately after the ignitor flow is terminated.

At the HAN-saturation point, approximately 86%, the chamber temperature approaches 750 C. This temperature is likely as high as can be achieved with HAN-decomposition alone. At 90% HAN-decomposition efficiency the predicted I_{sp} for a 75% binary HAN solution is approximately 145 seconds. With a high expansion ration nozzle, the approximate vacuum I_{sp} translates to approximately 200 seconds.

In order to burn at a higher temperature -- and achieve higher specific impulse -- an added fuel component is necessary. As described previously, this added performance potential comes at a cost as previous studies have shown that adding a fuel component has a stabilizing effect. This added chemical stability significantly increases the required energy input energy for thermal decomposition and significantly reduces the reaction rate for the solution.

Figure 18(b) plots the time required to vaporize all of the water in solution, and dissociate the HAN remaining after the water has vaporized. Figure 18(c)

plots the required chamber length to ensure at least 90% decomposition efficiency (from Eq. (25)). Clearly, the HAN-dissociation time is the primary driver here, as the water vaporization time is nearly two orders of magnitude faster. From the data plotted by Fig. 18(c), it appears that the 12.5 cm chamber length depicted in Fig. 15 is more than sufficient.

Calculations for the 12.5 N thruster operating at 1000 kPa chamber pressure produce similar results, with the primary exceptions being a longer HAN-dissociation time, and a slightly longer required chamber length. The length growth is significantly less than the increase in HAN-decomposition time as a result of the lower injector mass flow and the corresponding reduced injection velocity. It appears that this compensating-effect will allow the same chamber geometry to be used for both the *25 N* and *12.5 N* thruster designs.

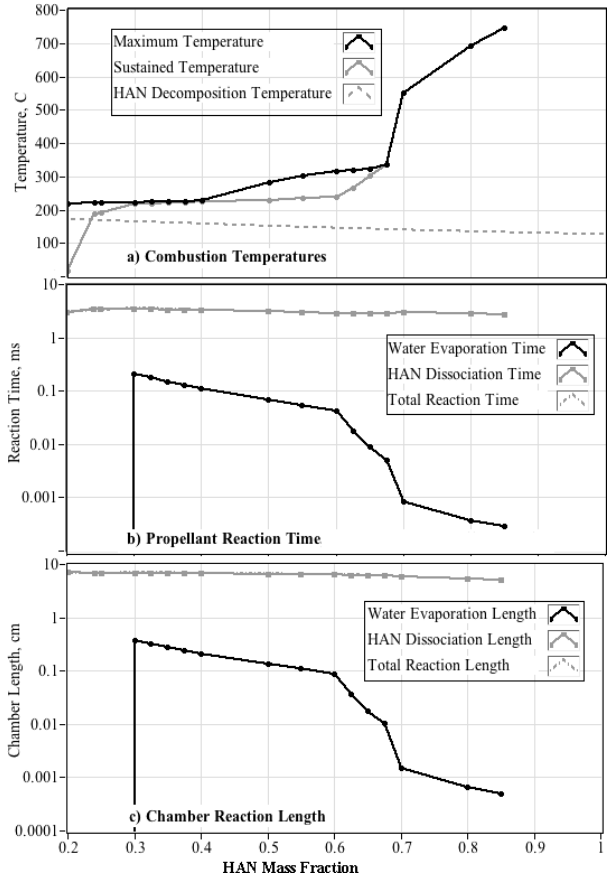

Figure 18. HAN Solution Decomposition Temperature and Time, and Chamber Reaction Length.

PROPOSED FUTURE WORK

Unfortunately, developmental testing has not been completed at the time of the publication of this document. Future papers will detail the results of the developmental tests. The thrust chamber of Figure 15 and the test apparatus of Figure 16 are currently being fabricated, assembled, and integrated. For the initial developmental tests a commercially available 24% HAN/H_2O binary solution* - the highest concentration that can be shipped as a non-hazardous material - will be evaluated. Testing will subsequently progress to increasingly higher HAN-solution concentrations prepared using existing facilities at USU. Future tests will also evaluate the effectiveness of the ignitor with ternary HAN/H_2O/fuel mixtures.

The top-level developmental test objectives are

1. Demonstrate repeatable and reliable thermal decomposition of binary *HAN/H_2O* solutions of varying concentration using a laboratory-weight system prototype with an integrated micro-hybrid igniter. Ambient, cold-soak, and initial-vacuum starts will be demonstrated.

2. Once the system effectiveness has been verified for binary HAN/H_2O solutions, a fuel component (either ethanol or methanol) will be added to evaluate igniter effectiveness with ternary propellant blends.

3. Results from these initial developmental tests will be used to identify critical system design parameters, and will be used to verify and adapt analytical models of the process.

4. Following the successful testing of the developmental thruster, the proven design tools will be used to optimize, build, and test flight weight prototypes sized for a 1-N fast-response, low minimum impulse-bit capability, and a 25-N long burn duration, higher total impulse capability.

5. Demonstrate that Robotic Manufacturing (RM) methods, including fused deposition modeling (FDM), and Direct Laser Metal Sintering (DMLS) can be used to fabricate flight weight components.

- *1-N and 25-N units will be optimized and fabricated using RM-methods.*
- *Proposed demonstration tests for flight-weight units.*
  - *Ambient, Cold-Soak, and Vacuum start/restart*
  - *Pulsed Operation, Minimum Impulse Bit Characterization/Optimization*
  - *Long Duration Burn*
  - *System Throttling*

Flight weight thrusters will be fabricated from inconel alloy or titanium, both materials that are compatible with HAN. Fabrication will leverage the DMLS process with the optimized 3-D CAD model created off-line and loaded onto the machine's

Sigma Aldridge catalog number 438235, Hydroxylammonium Nitrate Solution, 24% in H2O, 99.999%, http://www.sigmaaldrich.com/catalog/product/aldrich/438235?lang=en&region=US, [Retrieved 12 December 2012].

software. DMLS is ideally suited for constructing parts on the CubeSat scale. The DMLS machine fuses metal powder into a solid component using a high-powered 200-watt fiber optic laser. Components are built up additively in 20-micron layers and exhibit excellent mechanical properties equivalent to wrought materials. DLMS components have homogenous structure and exceptional surface quality.

Table 2: Prototype Thruster Design Parameters.

Ignitor	$P_{c,\ kPa}$	$D_{exit,\ cm}$	$C_{d\ exit}$	*# of Ignitors*	C^* *efficiency*	$\Delta T_{burnout}$, *s*	*O/F Ratio*	
	2100	3175	1.0	1	0.75	0.5	2	
HAN/H_2O Injector	$P_{c,\ kPa}$	$D_{port,\ cm}$	$C_{d\ port}$	*# of Ports*	*Decomposition Efficiency*	*Injectant Temperature, K*	*HAN Solution Injection Angle, deg*	
	2100	0.1	0.40	4	80%	294	45	
Combustion Chamber	$P_{amb,\ kPa}$ *(Design)*	*Chamber Length, cm*	$C_{d\ nozzle}$	*Chamber Volume, cm^3*	*Nozzle Diameter, cm* *A/A^* Nozzle*	θ_{exit} *Nozzle, deg.*	*Chamber Design Pressure, kPa*	*Ambient Thrust level, N*
	86	12	0.9	225	0.35	20	1000	12.5
					4.0		2000	25

Leveraging the capabilities of the robotic manufacturing process allows complex geometries to be created directly from the 3D CAD file without any additional tooling. Changing the component design is as simple as re-drawing the CAD file. Figure 19 shows 4 injector circuit designs that were DMLS-fabricated and tested at NASA Marshall Space Flight Center (MSFC). The evolutionary designs depicted in Fig. 19 were adapted from an original concept by modifying the existing CAD-file. The coaxial swirl injector design of Fig 19(c), with some slight modifications, is ideally suited as a drop-in replacement for the hand-fabricated injector depicted in Fig. 15. Under the authority of a Space Acts Agreement (SAA), MSFC will produce the needed DMLS flight weight components to support this project.

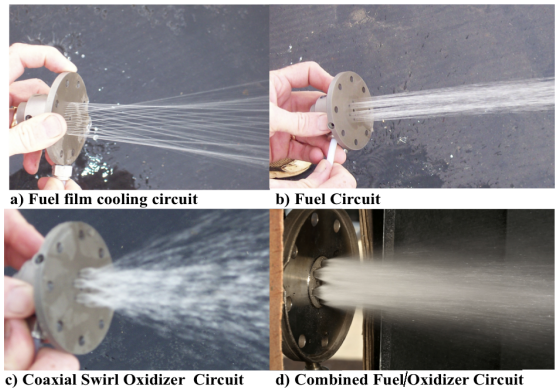

Figure 19. DMLS-Fabricated Titanium Injectors.

SUMMARY AND CONCLUDING REMARKS

This paper details the development and testing of a "green" monopropellant ignition system originally developed for hybrid rockets, but modified for Ionic-Liquid (IL) propellants. Numerical models have shown that the high total output enthalpy of the "micro-hybrid" exhaust gases provide more than sufficient energy to initiate thermal IL-propellant decomposition.

The design successfully ignited a 98-mm nitrous oxide/ABS hybrid rocket motor multiple consecutive times without hardware changeover or propellant replenishment. For initial proof-of-concept tests the high-voltage spark was provided using a hand-held TASER® stun-gun. Later tests used a precision high-voltage power supply with a current limiter. For the proof-of-concept ignition tests the power input started at less than 10 Watts for the initial burn, and then dropped to 2 Watts for the final burn. Total burn input energies averaged less than 5 joules.

The gas byproducts from the hydrocarbon-seeding process exceeded 2400 C with an output enthalpy rate of near 30 kW -- *an output-to-input power ratio of more than three orders of magnitude!* The mean total output energy for the igniter burns exceeded 20 kJ.

The required 5-Joule ignition input energy is contrasted with the ignition energy requirements for the 1-N IL-thruster flown by ESA on the Prisma flight experiment. For the Prisma flight test the sustained preheat load exceeded 8.5 watts, and consumed as much as 15,000 Joules of external power -- three orders of magnitude larger than the ignition technology presented in this paper. As an additional advantage, with the proposed design, catalyst bed survivability is not an issue. The only limit to the available igniter lifetime is the amount of seeding material that can be fit into the available volume.

The design also offers a smaller overall form factor at a considerably-reduced manufacturing cost. Unlike single-use "squib" pyrotechnic igniters, the system allows the gas generation cycle to be terminated and reinitiated on demand. The technique is fundamentally different from all other current or proposed ionic-liquid ignition solutions. The "micro-hybrid" igniter presented

here offers the potential to act as a "drop-in" replacement for existing *IL* catalyst beds. This application should allow the rapid infusion of IL-based propellants into a wide range of SmallSat missions.

References

1. Whitmore, Stephen A., "Hydrocarbon-Seeded Monopropellant Thruster," *Utah State University Technology Disclosure No. D12054*, April 12, 2012, *http://ipso.usu.edu/,* [Retrieved 15 July, 2012].

2. Anon., "Total Propulsion Solutions," *AeroJet, Redmond Operations*, 2006-H-3391, June 2007.

3. Choudhary G, IIansen H, Donkin S, Kirman C. 1997. Toxicological Profile for Hydrazines. *US Department of Health and Human Services Public Health Service Agency for Toxic Substances and Disease Registry (ATSDR),* Atlanta GA, pp. 1-224.

4. DeSain, John D., "Green Propulsion: Trends and perspectives," *Crosslink*, *http://www.aero.org/publications/crosslink/summer2011/04.html*, [Retrieved 21 March, 2012].

5. Anon., **"**Hazard Analysis of Commercial Space Transportation; Vol. 1: Operations, Vol. 2: Hazards, Vol. 3: Risk Analysis,**"** *U.S. Dept. of Transportation*, PB93-199040, Accession No. 00620693, May 1988.

6. Schmidt, E. W., *Hydrazine and its Derivatives: Perparation, Properties, Applications, Second Edition*, Vol. 2, Wiley-Interscience, 2001.

7. Haeseler, D., Bombelli, V., Vuillermoz, P., Lo, R., Marée, T., & Caramelli, F., "Green Propellant Propulsion Concepts for Space Transportation and Technology Development Needs," *ESA SP-557, Proceedings of the 2nd International Conference on Green Propellants for Space Propulsion*, Cagliari, Sardinia, Italy, 7-8 June 2004, p.4.1.

8. Bombelli, V., "Economic Benefits for the Use of Non-toxic Monopropellants for Spacecraft Applications, AIAA-2003-4783, *39th AIAA/ASME/SAE/ASEE Joint Propulsion Conference and Exhibit,* Huntsville, AL, 20-23, July 2003.

9. Meyer, M, Johnson L., Palaszewski, B., Goebel, D., White, D., and Coote, D., In-Space Propulsion Systems Roadmap, Technology Area 02 (TA02), "*Office of the Chief technologist, Space Technology Roadmaps*," April 2012, *http://www.nasa.gov/offices/oct/home/roadmaps/index.html*, [Retrieved 29 November, 2012].

10. Anon., "NASA Goes Green: NASA Selects Green Propellant Technology Demonstration Mission," *http://www.nasa.gov/home/hqnews/2012/aug/HQ_12-281_Green_Propellants.html*, [Retrieved 12 December 2012].

11. Hawkins, T. W., Brand, A. J., McKay, M. B., Tinnirello, M., " Reduced Toxicity, High Performance Monopropellant at the U.S. Air Force Research Laboratory," AFRL-RZ-ED-TP-2010-219, Edwards AFB CA, April 2010.

12. Wernimont, E. J., "System Trade Parameter Comparison of Monopropellants: Hydrogen Peroxide vs Hydrazine and Others," AIAA-2006-5235, *42nd AIAA/ASME/SAE/ASEE Joint Propulsion Conference & Exhibit*, Sacramento, CA, 9-12, July 2006.

13. Anon., "Occupational Health Guidelines for Hydrogen Peroxide," US Department of Health and Human Services Bulletin 0335, September, 1978, http:// *www.cdc.gov/niosh/docs/81-123/pdfs/0335.pdf*, [Retrieved 7 November 2012].

14. Venkatachalam, S., Santhosh, G., Ninan, K. N. , "An Overview on the Synthetic Routes and Properties of Ammonium Dinitramide (ADN) and other Dinitramide Salts". J. *Propellants, Explosives, Pyrotechnics*, Vol. 29, No. 3, March, 2004, pp.178–187.

15. Nagamachi, M. Y., Oliveira, J. I., Kawamoto, A. M., and Dutra, R., C., "ADN – The new oxidizer around the corner for an environmentally friendly smokeless propellant," *J. of Aerospace Technology Management*, Vol. 1, No. 2., December 2009, pp. 153-160.

16. Rheingold, A. L., Cronin, J. T., Brill, T. B., and Ross, F. K., "Structure of Hydroxylammonium Nitrate (HAN) and the Deuterium Homolog," *Acta Crystallographica*, Vol. 43, No. 1, 1987, pp. 402-404.

17. Pembridge, J. R., and Stedman, G., "Kinetics, Mechanism, and Stoicheiometry of the Oxidation of Hydroxylamine by Nitric Acid," J. *of Chemical Society, Dalton Transactions*, Issue 11, 1979, pp. 1657-1663.

18. Handy, S., ed., *Applications of Ionic Liquids in Science and Technology*, InTech Publishing, New York, 2011, Chapt. 21, also available online *http://www.intechopen.com/books/applications-of-ionic-liquids-in-science-and-technology,* [Retrieved 7 November 2012].

19. Anon., "SRI International," URL: http://www.sri.com/about, [Retrieved 27 September 2012].

20. Bottaro, J.C., Penwell, P.E., Schmitt, R.J., 1997, "1,1,3,3-Tetraoxo - 1,2,3-Triazapropene Anion, a New Oxy Anion of Nitrogen: The Dinitramide Anion and Its Salts", *J. Am. Chem. Soc*., Vol. 119, pp. 9405-9410.

21. Anon., A-ZET.org, "ECAPS, Moog and ATK Announce Partnership to Bring High Performance Green Propulsion (HPGP) Technology to the US Space Propulsion Market," *http://www.a-zet.org,* [Retrieved 27 September 2012].

22. Goldstein, Edward, "The Greening of Satellite Propulsion," *Aerospace America*, February 2012, pp. 26-28.

23. Pokrupa, N., Anglo, K., and Svensson, O., "Spacecraft System Level Design with Regards to Incorporation of a New Green Propulsion System," AIAA-2011- 6129, *46th AIAA/ASME/SAE/ASEE Joint Propulsion Conference and Exhibit,* San Diego, CA, July 31-Aug 3, 2011.

24. Persson, M., Anflo, K., and Dinardi, A., "A Family of Thrusters For ADN-Based Monopropellant LMP-103S," *AIAA-2012-3815, 48th AIAA/ASME/SAE/ASEE Joint Propulsion Conference & Exhibit,* Atlanta Georgia, 30 July - 01 August 2012, 2012.

25. Klein, N., and Stiefel, L., ed. "Liquid Propellants for Use in Guns," *Gun Propulsion Technology, Progress in Astronautics and Aeronautics*, Vol. 109, AIAA, Washington, D.C., 1988, Chapter 14.

26. Anon., "Liquid Propellant 1846 Handbook," Jet Propulsion Laboratory, U.S. Department of the Army*,* ARDEC, Picatinny *Arsenal,* NJ, July, 1994.

27. Freedman, E., and Stiefel, L., ed. "Thermodynamic Properties of Military Gun Propellants", *Gun Propulsion Technology, Progress in Astronautics and Aeronautics*, Vol. 109, AIAA, Washington, D.C., 1988, Chapter 5.

28. JanKovsky, R. S., HAN-Based Monopropellant Assessment for Spacecraft," NASA TM 107287, (Also AIAA-96-2863), *32nd AIAA/ASME/SAE/ASEE Joint Propulsion Conference and Exhibit*, Lake Buena Vista, FL, July 1-3, 1996.

29. Decker, M.M.; Klein N.; Freedman, E.; Leveritt, C.S.; Wojciechowski, J.Q.: "HAN- Based Liquid Gun Propellants: Physical Properties," BRL-TR-2864, 1987.

30. Meinhart, D., "Selection of Alternate Fuels for HAN-BASED Monopropellants," *27th JANAFF PDCS and 16th S&EPS Joint Meeting*, CPIA Pibl. 674, Vol. 1, April 1998, Pp. 143-147.

31. Hurlbert, E., Applewhite, J., Nguyen, T., Reed, B., Zhang, B., and Wang, Y., "Nontoxic Orbital Maneuvering and Reaction Control Systems for Reusable Spacecraft," *Journal of Propulsion and Power*, Vol. 14, No. 5, 1998, pp. 676-687.

32. Anon., " Department of Defense Interface Standard, Eletromagnetic Environmental Effects requirements for Systems, MIL-STD-464, http:// *www.tscm.com/MIL-STD-464.pdf,* [Retrieved 8 October 2012].

33. Bonanos, A. M., Schetz, J. A., O'Brien, W. F., and Goyne, C. P., "Dual-Mode Combustion Experiments with an Integrated Aeroramp-Injector/Plasma-Torch Igniter", *Journal of Propulsion and Power*, Vol. 24, No. 2, March-April, 2008, pp. 267-273.

34. Anon., "SpaceX, Updates: February 2005-May 2005," Space Exploration Technologies, *http://www.spacex.com/updates_archive.php?page=0205-0505,* [Retrieved 11 October, 2012].

35. Persson, M., Anflo, K., and Dinardi, A., "A Family of Thrusters For ADN-Based Monopropellant LMP-103S," AIAA-2012-3815, *48th AIAA/ASME/SAE/ASEE Joint Propulsion Conference & Exhibit*, 30 July - 01 August 2012, Atlanta, Georgia, 2012.

36. Zube, D., Christofferson, S., Wücherer, E., and Reed, B., "Evaluation of HAN-Based Propellant Blends," 2003, AIAA Paper

2003-4643, *39th AIAA/ASME/SAE/ASEE Joint Propulsion Conference*, Huntsville, AL, 20-23 July, 2003.

37. Courthéoux, L., Eloirdi, R., Rossignol, S., Kappenstein, C., and Duprez, D., "Catalytic Decomposition of HAN-Water Binary Mixtures," *AIAA-2002-4027, 38th AIAA/ASME/SAE/ASEE Joint Propulsion Conference & Exhibit*, Indianapolis IN, 7-10 July 2002.

38. Oommen, C., Rajaraman, S., Chandru, R. A., Rajeev, R., "Catalytic Decomposition of Hydroxylammonium Nitrate Monopropellant," 2011 International Conference on Chemistry and Chemical Process, IPCBEE vol.10, Singapore, 2011, *http://www.ipcbee.com/vol10/39-V10034.pdf, [Retrieved 4 October 2012*].

39. Ren, X., Wang, A., Xu, D., Cong, Y., Wang, X., and Zhang, T., "Catalytic Decomposition of HAN-Based Monopropellant at Room Temperature over Ir/SiO2 Catalyst," SP-635, Ionic Liquids Session, "*The 3rd International Conference on Green Propellant for Space Propulsion*," Futuroscope, France, 17-29 September, 2006.

40. Ren, X., Li, M., Wang, A., Li, L., Wang, X., and Zhang, T., "Catalytic Decomposition of Hydroxyl Ammonium Nitrate at Room Temperature," *Chinese Journal of Catalysis*, Vol. 28, No. 1, 2007, pp. 1-2, *http://www.chxb.cn/EN/Y2007/V28/I1/1*, [Retrieved 4 October 2012].

45. Chang, Y. P., and Kuo, K. K., "Assessment of Combustion Characteristics and Mechanisms of Hydroxylammonium Nitrate-Based Liquid Monopropellant," *Journal of Propulsion and Power*, Vol. 18, No. 5, Sept-Oct, 2002.

41. Risha, G. A., Yetter, R. A. & Yang, V. (2007). Electrolytic-induced decomposition and ignition of HAN-based liquid monopropellants," *International Journal of Energetic Materials & Chemical Propulsion*, Vol. 6, No. 5, pp. 575-588,

42. Meng, H., Khare, P., Risha, G. A., Yetter, R. A., and Yang, V., "Decomposition and Ignition of HAN-Based Monopropellant by Electrolysis," AIAA-2009-451, *The New Horizons Forum and Aerospace Exposition,* Orlando, Florida, 5 - 8 January 2009.

43. Khare, P., "Decomposition and Ignition of HAN-Based Monopropellants by Electrolysis," MS Thesis," Pennsylvania State University Graduate School, College of Engineering, May 2009.

44. Kuo, B. H., "A Study on the Electrolytic Decomposition of HAN-Based Propellants for Microthruster Applications," *MS Thesis*, Pennsylvania State University Graduate School, College of Engineering, December 2010.

45. Wu, M. H., Yetter, R., and Yang, V., "Development and Characterization of Ceramic Micro Chemical Propulsion and Combustion Systems," AIAA-2008-966, 46th AIAA Aerospace Sciences Meeting and Exhibit AIAA 2008-966, Reno, Nevada, 7 - 10 January 2008.

46. Meinhardt, D., Brewster, G., Christofferson, S., Wucherer, E.," Development and Testing of New HAN-based Monopropellants in Small Rocket Thrusters," *AIAA-98-4006, 34th AIAA/ASME/SAE/ASEE Joint Propulsion Conference and Exhibit,* Cleveland, OH, July 13-15, 1998.

47. Meinhardt, D., Christofferson, S., and Wucherer, E.," Performance and Life Testing of Small HAN Thrusters," *AIAA-98-4006, 35th AIAA/ASME/SAE/ASEE Joint Propulsion Conference and Exhibit,* Los Angeles, CA, June 20-24, 1999.

48. Peterson, Z. W., Eilers, S., A., and Whitmore, S. A., "Analytical and Experimental Comparisons of HTPB and ABS as Hybrid Rocket Fuels," AIAA-2011-5909, *47th AIAA/ASME /SAE/ASEE Joint Propulsion Conference & Exhibit, San Diego CA, 31 July-3 August 2011.*

49. Shugg, W. T., *Handbook of Electrical and Insulating Materials*, Van Nostrand Reinhold, New York, 1986.

50. Anon., "High Power 8C-30C Series, Single Output High Voltage DC/DC Modules," UltraVolt, Inc., URL: *http://www.ultravolt.com/uv_docs/HP8C-30CDS.pdf*, [Retrieved 9 October 2012].

51. Rheingold, A. L., Cronin, J. T., Brill, T. B., and Ross, F. K., "Structure of Hydroxylammonium Nitrate (HAN) and the Deuterium Homolog," *Acta Crystallographica*, Vol. 43, No. 1, 1987, pp. 402-404.

52. Pembridge, andJ. R., Stedman, G., "Kinetics, Mechanism, and Stoicheiometry of the Oxidation of Hydroxylamine by Nitric Acid," *J. of Chemical Society,* Dalton Transactions, Issue 11, 1979, pp. 1657-1663.

53. Gordon, S., and McBride, B. J., "Computer Program for Calculation of Complex Chemical Equilibrium Compositions and Applications," NASA RP-1311, 1994.

54. Eilers, S. D., and Whitmore, S. A., "Correlation of Hybrid Rocket Propellant Regression Measurements with Enthalpy-Balance Model Predictions," *Journal of Spacecraft and Rockets*, Vol. 45, No. 4, September/August, 2008, pp. 1010-1020.

55. Schoppelrei, J. W., Kieke, M. L., Brill, T. B., "Spectroscopy of Hydrothermal Reactions. 2. Reactions and Kinetic Parameters of [NH3OH]NO3 and Equilibria of (NH4)2CO3 Determined with a Flow Cell and FT Raman Spectroscopy," *Journal of Physical Chemistry*, Vol. 100, No. 18, 1996, pp.7463–7470.

56. Sasse, R. A., "Thermal Characteristics of Concentrated HydroxylAmmonium Nitrate Solutions," US Army Ballistics Research Laboratory, Report BRL-MR-3561, March 1988.

57. Lemmon, E.W. and M.O. McLinden, "NIST Standard Reference Database 23: NIST Reference Fluid Thermodynamic and Transport Properties, Version 7.0 Beta," National Institute of Standards and Technology, Gaithersburg, 2001; *http://www.nist.gov/srd/nist23.htm.* [Retrieved 04 December, 2008].

58. Hill, T. L., *Statistical Thermodynamics*, Addison-Wesley, Reading (1960), p. 280

59. Kounalakis, M. E., and Faeth, G. M., " Combustion of Han-Based Liquid Monopropellants Near the Thermodynamic Critical Point," *J. Combustion and Flame*, Vol. 74, No. 1. 1988, pp. 179-192.

60. Harlow, D. G., Felt, R. E., Agnew, S., Barney, S., McKibben, J. M., Garber, R, and Kewis, M., "Technical Report on Hydroxylamine Nitrate," U.S. Department of Energy, DAE/EH-0555, February 1998.

61. Lee, H. S., and Litzinger, T. A., " Chemical Kinetic Study of HAN Decomposition," *Combustion and Flame*, Vol. 135, No. 1., 2003, pp. 151-169.

62. Pan, Y. Z., Yu, Y. G., Zhou, Y. H., ands Ly, X., " Measurement and Analysis of the Burning Rate of HAN-Based Liquid Propellants," *J. Propellants Explosives &* Pyrotechnics, Vol. 37, No. 3, 2012, pp. 439 – 444.

63. Vosen, S. R., " Concentration and Pressure Effects on the Decomposition Rate of Aqueous Hydroxylammonium Nitrate Solutions," *Combustion Science and Technology*, Vol. 68, No. 4-6, 1989, pp. 85-99.

64. Kondrikov, B. N. et al., "Burning of Hydroxylammonium Nitrate," *J. of Combustion, Explosion, and Shock Waves*, Vol. 36, No.1, Jan. 2000, pp.135-145.

65. Katsumi, T., and Hori, K., " Combustion Wave Structure of Hydroxylammonium Nitrate Aqueous Solutions," AIAA 2010-6900, *46th AIAA/ASME/SAE/ASEE Joint Propulsion Conference & Exhibit*, 25 - 28 July 2010, Nashville, TN.

66. Lefebvre, A. H., "*Atomization and Sprays*," Taylor & Francis, Inc., New York, 1989, pp. 1-75.

67. Schick, R. J., "Understanding Drop Size," Spray Analysis and Research Services, Spray Technology Reference Guide, *http://www.teejet.com/media/40081/understanding%20drop%20size.pdf*, [Retrieved 26 March 2013].

68. Langmuir, I., "The Vapor Pressure of Metallic Tungsten," *Physical Review*, Vol. 2., No. 5, Nov. 1913, pp 329-342.

69. Wei, C., Rogers, W. J., Mannan, M. S., "Thermal Decomposition Hazard Evaluation of Hydroxylamine Nitrate," *J. of Hazardous Materials*, Vol. 130, N0. 1, pp. 163-168.